JOURNAL OF GEOPHYSICAL RESEARCH, VOL. 112, B05311, doi:10.1029/2006JB004622, 2007

Regional mapping of the crustal structure in southern California from receiver functions

Z. Yan[1,2] and R. W. Clayton[1]

Received 6 July 2006; revised 8 November 2006; accepted 16 January 2007; published 25 May 2007.

[1] Lateral variations of the crustal structure in southern California are determined from receiver function (RF) studies using data from the Southern California Seismic Network broadband stations and Los Angeles Regional Seismic Experiment surveys. The results include crustal thickness estimates at the stations themselves, and where possible, cross sections are drawn. The large-scale Moho depth variation pattern generally correlates well with the current status of the Mesozoic batholith: Deep Moho of 35–39 km is observed beneath the western Peninsula Ranges, Sierra Nevada, and San Bernardino Mountains, where the batholith is relatively intact, and shallow Moho of 26–32 km is observed in the Mojave Desert, where the batholith is highly deformed and disrupted. High-resolution lateral variations of the crustal structure for individual geographic provinces are investigated, and distinctive features are identified. The crustal structure is strongly heterogeneous beneath the central Transverse Ranges, and deep Moho of 36–39 km is locally observed beneath several station groups in the western San Gabriel Mountains. Moho is relatively flat and smooth beneath the western Mojave Desert but gets shallower and complicated to the east. Anomalous RFs are observed at two stations in the eastern Mojave Desert, where a Moho step of ~8–10 km is found between the NW and SE back-azimuthal groups of station DAN in the Fenner Valley. Asymmetric extension of the Salton Trough is inferred from the Moho geometry. Depth extension of several major faults, such as the San Andreas Fault and San Gabriel Fault, to the Moho is inferred.

Citation: Yan, Z., and R. W. Clayton (2007), Regional mapping of the crustal structure in southern California from receiver functions, *J. Geophys. Res.*, *112*, B05311, doi:10.1029/2006JB004622.

1. Introduction

[2] Lateral variations of the crustal structure are of fundamental importance to understanding of the current status of the lithosphere, and the correlation of the subsurface structure with the surficial geology can provide important insight into the coupling relationship between the upper and the lower crust and thus the strength of the lower crust. Surficial geology in the southern California indicates that large-scale deformations have occurred during and after the transition of the plate boundary from a convergent one to a strike-slip one. Examples of the deformations include the block rotation of the central and the western Transverse Ranges, the opening of the Gulf of California, and the large-scale extension in the Basin and Range province. Various blocks in southern California behave very differently during the evolution of the plate boundary: Sierra Nevada, the Great Valley, and the Peninsula Ranges remain almost as intact blocks, while the continental crust of the Basin and Range province, including the Mojave Desert, is strongly extended, highly deformed, and disrupted. Thus southern California provides a very good natural laboratory to investigate the response of the continental crust to the different deformation styles.

[3] Extensive efforts have been made to investigate the crustal structure in southern California. These include an early local refraction and teleseismic P wave traveltime delay studies by *Hadley* [1978] and *Hadley and Kanamori* [1977, 1979], who built a standard regional model for southern California and found a high-velocity body in the upper mantle beneath the Transverse Ranges. A kinematic model which proposes that the crust and the upper mantle are decoupled across the southern California and that the plate boundary is shifted to the east beneath the Eastern California Shear Zone in the upper mantle was inspired by the fact that this upper mantle high-velocity body is continuous across the San Andreas Fault and its spatial extension to the active Helendale-Lenwood fault zone [*Hadley and Kanamori*, 1979]. This high-velocity anomaly was further refined by tomography studies and its spatial dimension was constrained to be ~80 km in N-S direction, ~150 km in W-E direction and extends to ~200–250 km in depth with a 2–3% P velocity anomaly [*Humphreys et al.*, 1984; *Humphreys and Clayton*, 1990; *Kohler*, 1999]. Common explanation for this high upper mantle velocity body is

[1]Seismological Laboratory, California Institute of Technology, Pasadena, California, USA.
[2]Now at WesternGeco, Houston, Texas, USA.

0148-0227/07/2006JB004622$09.00

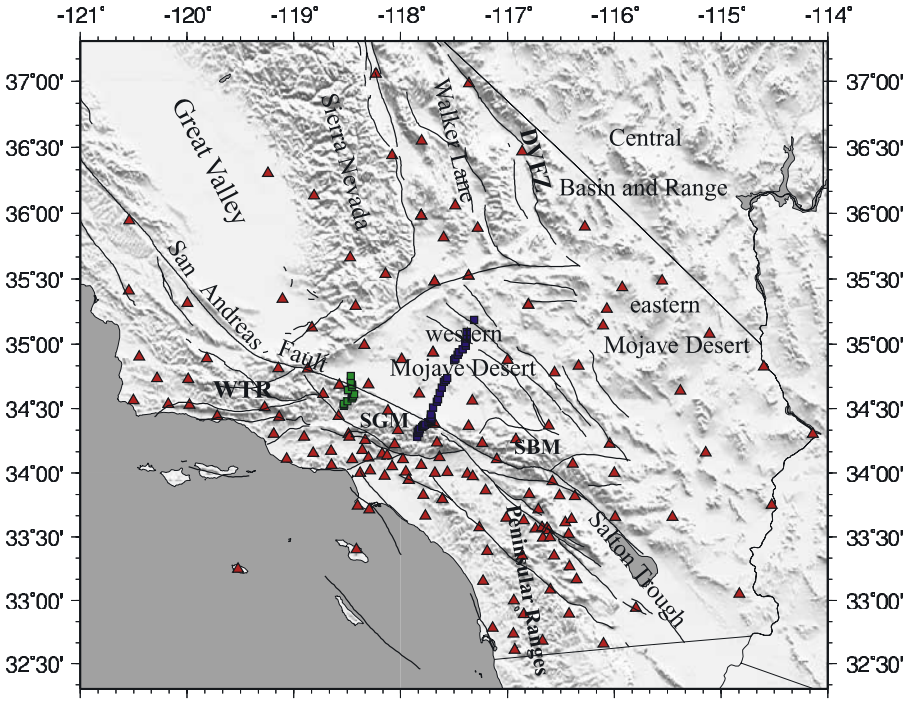

Figure 1. Map showing the stations used in this study, along with major faults in southern California [*Jennings and George*, 1994]. Red triangles are SCSN stations, blue squares are LARSE I stations, and green squares are LARSE II stations. WTR, Western Transverse Ranges; SGM, San Gabriel Mountains; SBM, San Bernardino Mountains; DVFZ, Death Valley fault zone.

that it is caused by subcrustal lithosphere downwelling [*Humphreys and Hager*, 1990; *Kohler*, 1999]. For the involvement of the crust, however, different kinematic models have been proposed and the two end-members are kinematic decoupling of the crust and upper mantle, in which the crust remains flat [*Humphreys and Hager*, 1990; *Humphreys*, 1995], and strong coupling between the crust and the upper mantle, in which the crust deepens accordingly [*Houseman et al.*, 2000; *Kohler*, 1999]. The key to solving this mystery lies in the crustal thickness beneath the San Gabriel Mountains, which is still in debate.

[4] The studies that support shallow Moho beneath the San Gabriel Mountains include *Zhu and Kanamori*'s [2000] teleseismic receiver function (RF) studies from 65 TriNet broadband stations, *Zhu*'s [2000] teleseismic receiver function studies from the Los Angeles Regional Seismic Experiment (LARSE) I passive stations, and *Richards-Dinger and Shearer*'s [1997] PmP–P differential time studies. These studies all infer a shallow crust of 28–31 km for the central Transverse Ranges. In contrast, *Kohler and Davis* [1997] inferred the existence of a deep root of 40 km centered at the San Andreas Fault from teleseismic traveltime studies of the LARSE I passive stations. A feature that further complicates the interpretation is that two interfaces are apparent in *Zhu*'s [2000] teleseismic receiver function image along the LARSE I line. *Zhu* [2000] picked the shallower one at 25–29 km to be the Moho, while others argue that the deeper interface at around 40 km with slightly smaller amplitude could be the Moho instead. All these indicate that further study of the crustal structure beneath the San Gabriel Mountains is needed to resolve the controversy.

[5] Broadband stations in southern California (Figure 1) have been nearly tripled since 2001 after *Zhu and Kanamori*'s [2000] regional RF study. Also with this previous study, the RFs from all back azimuths were stacked together to give an estimate of the averaged Moho depth beneath a station, while large differences in the Pms arrival time among the different back-azimuthal groups are observed for most stations in the San Gabriel Mountains and some stations in other geographic provinces. Events from different directions pierce the Moho at locations that are separated by as much as 15–20 km laterally, so the difference in the Pms arrivals among the different back-azimuthal groups can be exploited to find rapid lateral variations in the crustal structure.

[6] The RF method has the advantage of providing a very good localized estimate of the crustal structure beneath a station. In this study, we will take advantage of this property to develop a relatively high-resolution regional Moho depth map for southern California. We will exploit the densely distributed broadband stations in southern California, and the large number of suitable teleseismic events to increase the lateral resolution, especially beneath individual stations, by stacking the RFs over several restricted back-azimuthal ranges for each individual station. This will allow us to identify the lateral variations of the structure beneath individual stations, which is particularly important for stations near major faults. Compared with other techniques, such as wide-angle reflection and refraction studies, the local and relative timing nature of the RF method makes the results less dependent on the lateral and vertical variations in the velocity structure. The estimate only depends weakly on the average crustal P velocity and an uncertainty in the

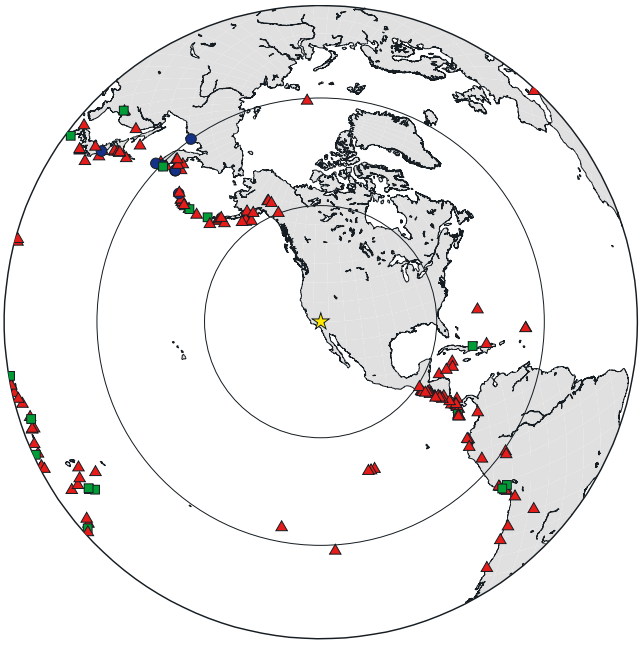

Figure 2. Azimuthal equal-area projection of the locations of teleseismic events used by this study, which includes 144 events for the SCSN stations (red triangles), 12 events for the LARSE I survey (blue circles), and 17 events for the LARSE II survey (green squares). The yellow star in the center represents the SCSN station TA2 at Table Mountain, Wrightwood. The distances of 30°, 60°, and 90° are shown by the concentric circles.

average Vp of 0.1 km/s will result in an uncertainty of less than 0.5 km in the Moho depth for a 30 km thick crust [*Zhu and Kanamori*, 2000]. However, the relative timing nature of RF makes them highly dependent on the average crustal Vp/Vs ratio [*Zhu and Kanamori*, 2000]. In this paper, we use the stacking algorithm developed by *Zhu and Kanamori* [2000], which uses multiples of the Pms phase to estimate the crustal thickness and Vp/Vs ratio.

2. Data and Analysis

[7] To produce a detailed map of lateral variations in the crustal structure of southern California, 164 nonbasin broadband stations of the Southern California Seismic Network (SCSN) were used along with the stations from the passive component of the LARSE I [*Kohler and Davis*, 1997; *Zhu*, 2000] and LARSE II [*Fuis et al.*, 2001; *Zhu*, 2002] surveys. Locations of the SCSN stations and the LARSE surveys are shown in Figure 1. A total of 144 teleseismic earthquakes from 2001 recorded by the SCSN stations with magnitude larger than 5.5, and a distance range between 30° and 95° were used (Figure 2). The actual numbers of events for individual stations vary from 20 to 140, depending on the signal-to-noise level of the waveform data, and the recording period of the station. Over the deployment period, the LARSE I stations recorded 12 good events from the NW back azimuth. The LARSE II recorded 3–6 high signal-to-noise ratio events from SW and SE, respectively (Figure 2).

[8] Teleseismic waveform data with signal-to-noise ratios higher than 3 were selected. The records were time windowed to 90 s, starting 15 s before the P wave onset, band-pass-filtered (0.02–2 Hz), and the two horizontal components were rotated to the radial and tangential directions. Two types of deconvolution techniques were used to deconvolve the vertical component from the radial and tangential components. Because of the existence of low-frequency noise in the LARSE I and LARSE II data sets, the frequency domain deconvolution [e.g., *Langston*, 1977, 1989; *Owens and Zandt*, 1985; *Ammon et al.*, 1990] using spectral division with water levels 0.001, 0.01, and 0.1 and Gaussian filter parameters of 2.5 and 5.0 were used. Selection of the water level and Gaussian parameters for each record is determined by the presignal noise levels. For RFs with sufficiently low presignal noise levels, the RF with the lowest water level and higher Gaussian parameter is selected. The iterative time domain deconvolution technique, which has the advantage of generating zero presignal noise [*Ligorria and Ammon*, 1999; *Kikuchi and Kanamori*, 1982], was used for the broadband SCSN data. RFs generated by both deconvolution techniques have been studied in detail by this work and previous studies [*Ligorria and Ammon*, 1999], and no difference in the major pulses is observed between the results of the two methods for high signal-to-noise ratio waveform data. Refer to *Ligorria and Ammon* [1999] for details.

[9] The signal-to-noise ratio is increased by stacking the RFs grouped by their conversion points (back azimuth). Although the variation of the RFs over the whole back-azimuthal range is large, they are very similar to each other within a limited azimuthal range (see Figure 3). The RFs for each station are divided into nine back-azimuthal groups, and the grid search stacking algorithm of *Zhu and Kanamori* [2000] was applied to groups with more than five RFs to get an estimate on the Moho depth, H, and the Vp/Vs ratio, κ, at the surface projection of the conversion point at the Moho. The conversion point is normally 7–10 km away (in the back-azimuth direction) from the receiving station, depending on the ray parameter. Since estimates of the Moho depth depend only weakly on the averaged crustal P velocity, it is assumed to be 6.3 km/s for all stations for simplicity and consistency. The search range of H and κ for most station groups are $H \in [25, 45]$, and $\kappa \in [1.65, 1.90]$. In regions where the Moho depth deviates substantially from 28 to 38 km, the searching range for H is modified accordingly. For example, the search range for H is 15–30 km for stations close to the Salton Sea. Uncertainty estimates for the grid search is taken to be the 95% maximum contour for the purpose of distinguishing RF groups with relatively well-developed multiples. Comparing with the uncertainty estimation method of *Zhu and Kanamori* [2000], this estimate has the advantage of being able to determine how well developed the multiples are from the geometry of the contours, which in turn will be used to select well-constrained data points.

[10] When the 95% contour of the (H, κ) grid search is broad in any direction (Figure 4) or has more than one local maximums, it indicates that either the amplitude of the multiples is too small to be distinguishable from background noise or that several reverberations exist in the data and it is difficult to tell which one is the true multiple. In both cases, the grid search algorithm does not work since

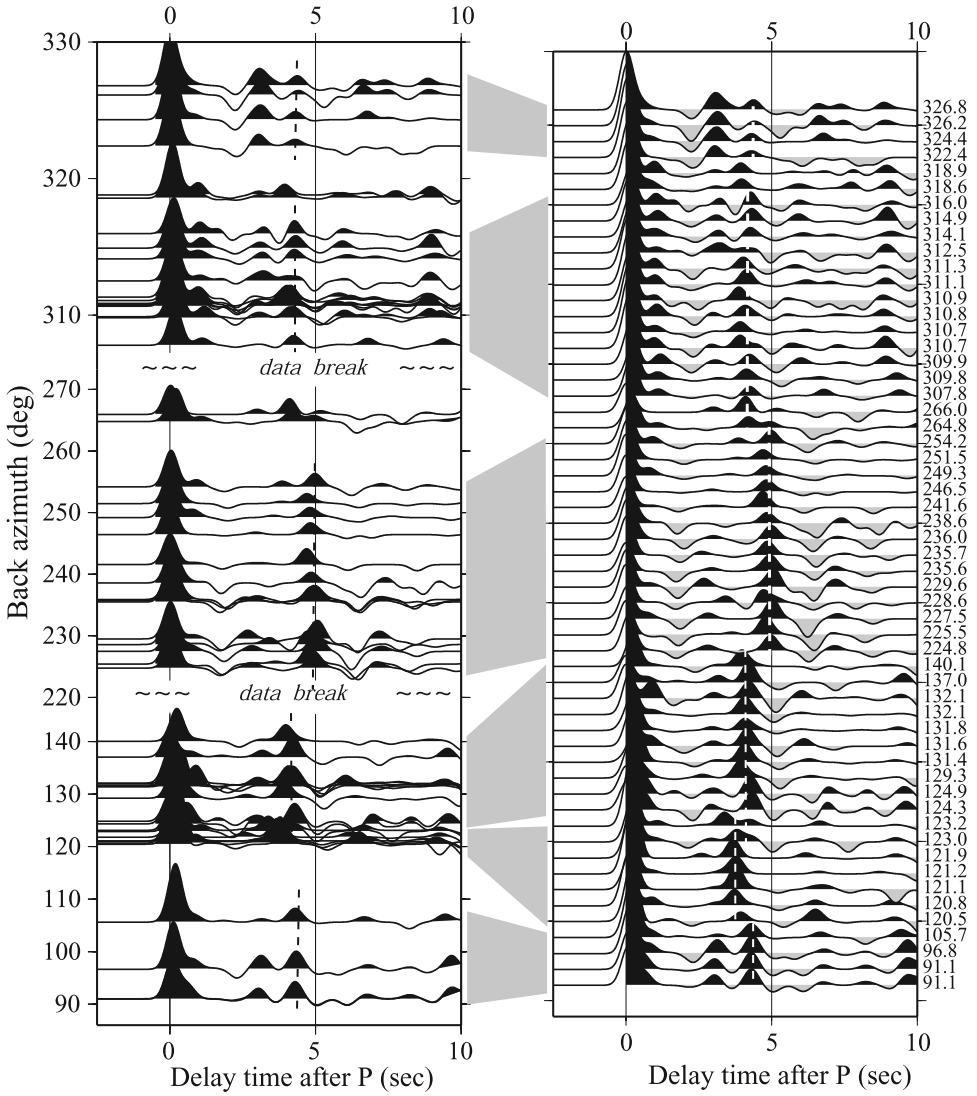

Figure 3. Receiver Functions for station VCS (Vincent Substation). (left) RFs as a function of back azimuth, and (right) RFs evenly spaced but in the order of increasing back azimuth from bottom to top. Note the late Pms arrivals (4.8 s) for events from SW and earlier arrivals of 3.8–4.2 s for those from other directions.

well-developed multiples are required for the grid search to be successful. An example of a successful stacking group is show in Figure 5, which shows clear PpPms and PsPms multiples though the PsPms multiples are a little bit delayed due to minor lateral variations in the crustal structure. The selection criteria to distinguish the well-constrained data points are: only one 95% contour exists, uncertainty range for κ is less than 0.15, and 100% of the polarities for the primary phase, more than 50% of the polarities for both multiples are correct. Only station groups that meet the above criteria are included in the regional Moho depth mapping of Figure 6. For groups that fail these criteria, but have prominent and consistent Pms phases, such as the SW back-azimuthal group of VCS (Figure 4), the averaged stack traces are included in the profiles and are migrated into the ''pseudodepth'' domain using the iasp91 model for consistency. For the LARSE I and LARSE II passive data, continuity of the Moho interface with nearby stations is assumed, and RFs from neighboring stations were referenced in constraining the Pms pick when multiple Ps phases exist between 3 and 5.5 s.

[11] In summary, procedures for this RF study are as follows. (1) For all the available waveforms for each event, data were selected according to the signal-to-noise ratio, and only stations with signal-to-noise ratios higher than 3.0 were retained. (2) The vertical component is deconvolved from the radial and tangential components to get the radial and tangential RFs for each station of each event. (3) All the available RFs for each station from different events were then divided into nine groups according to back-azimuth, and the grid search algorithm is applied to groups with more than five events to get a point estimate the H and κ. (4) Groups with distinguishable multiples were selected for the Moho depth mapping. (5) The averaged stack traces of groups with

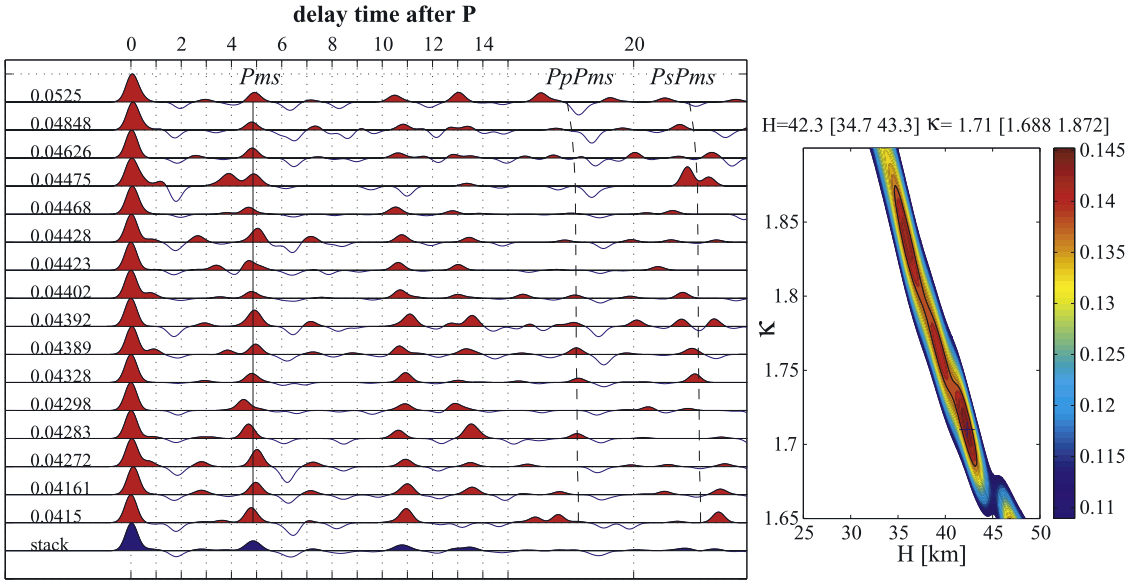

Figure 4. [H, κ] domain grid search of the SW group of VCS. (left) Individual RF traces for this group sorted according to the ray parameter. The predicted arrival times of the primary phase (Pms) and the two multiples (PpPms and PsPms) for the picked (H, κ) are marked by the solid and the dashed lines. The multiples for this group are not well developed, which explains why the [H, κ] domain grid search is not successful. (right) Contour map of the weighted summation function [*Zhu and Kanamori*, 2000]. The black cross is the picked (H, κ), that maximize the summation function, and the black line is the 95% maximum contour, which represents the uncertainty estimate for the picked (H, κ). Note that the 95% contour is very broad in the κ direction.

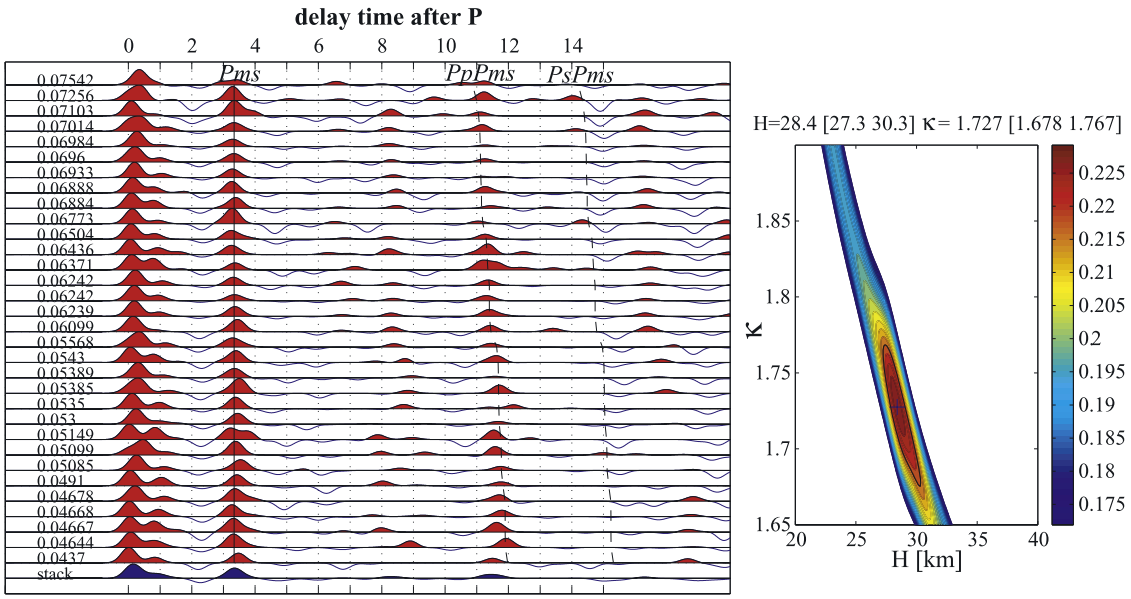

Figure 5. [H, κ] domain grid search of the NW group of PAS. Similar to Figure 4, except this is an example of successful stacking group. For this group, the estimated Moho depth is 28.4 km, with uncertainty range [27.3, 30.3]. Vp/Vs ratio, κ, is 1.727, with uncertainty range [1.678, 1.767]. Note the Vp/Vs ratio is not very well constrained with this method. Individual RF traces are shown in Figure 5 (left) with arrival times for the three phases marked. Note that the Pms and PpPms are very well determined. True arrival times of the PsPms phase are slightly delayed than those predicated, probably due to small lateral heterogeneity in the crustal structure.

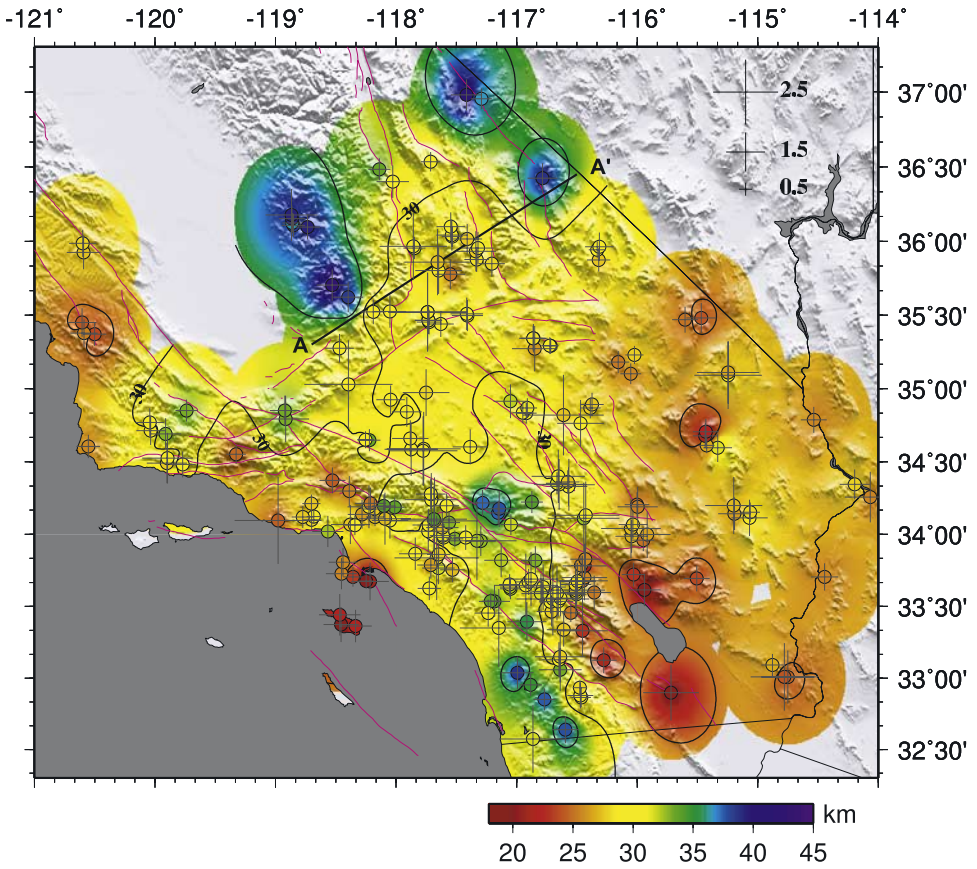

Figure 6. Interpolated Moho depth map from the selected data points that show distinguishable multiples. Each circle represents one data point and is located at the P-to-S conversion point from a 30-km-deep interface as computed from the averaged ray parameter and back azimuth of the corresponding stacking group. An inverse distance algorithm is used to interpolate the data points within a 45 km circle of each data point. Crosses at each circle represent the uncertainty of the Moho depth estimation, and the uncertainty scale is shown at the upright corner. Moho contours of 25, 30, and 35 km are also shown. The Moho depths have been corrected for station elevations. The black line AA′ is the Sierra Nevada profile shown in Figure 7.

prominent primary phases were selected to construct RF cross sections for the relatively well-sampled areas.

3. Results and Discussions

[12] A total of ~250 stacking groups with well-developed multiples were selected from more than 700 stacking groups for the SCSN data. None of the LARSE I or LARSE II passive station groups were selected due to the small number of available events or no distinguishable multiples. The Moho depth map derived from these well-constrained data points is shown in Figure 6, and the estimated Moho depth, Vp/Vs ratio, etc., are listed in Table S1 in the auxiliary material.[1] A large portion of the station groups in the western Peninsula Ranges, Mojave Desert, Southern Sierra, and Walker Lane is are selected due to the relative smoothness of the Moho interface in these areas. Most station groups in the western San Gabriel Mountains do not meet the selection criteria because of strong lateral heterogeneity in the crustal structure, and they are thus excluded from the map. Stations in the Great Valley, Salton Trough, and the Los Angles basin were not included because of complications to the waveforms/RFs from the low-velocity sedimentary cover.

[13] The imaged Moho depth map shares similar broad-scale features with those reported in other studies [*Cheadle et al.*, 1986; *Li et al.*, 1992; *Richards-Dinger and Shearer*, 1997; *Zhu and Kanamori*, 2000]. Thinner crust of 19–22 km and 25–27 km is observed close to the Salton Trough, and the eastern Mojave Desert, respectively. The Moho is relatively flat in the western Mojave Desert and the southern Walker Lane area with a depth of 28–31 km. Thick crust of 34–38 km is observed beneath the western Peninsula Ranges, the San Bernardino Mountains, and the western Sierra Nevada Mountains. However, compared with previous studies, the density of RF station groups enables us to provide more details on the lateral variations of the crustal structure. In the following, results will be discussed according to geographical provinces. RFs along several cross sections, where the station groups are densely distributed, are presented.

3.1. Southern Sierra Nevada and the Walker Lane Belt

[14] Substantial variations in the Moho depth are imaged beneath the southern Sierra Nevada and the nearby Walker

[1] Auxiliary materials are available at ftp://ftp.agu.org/apend/jb/2006jb004622.

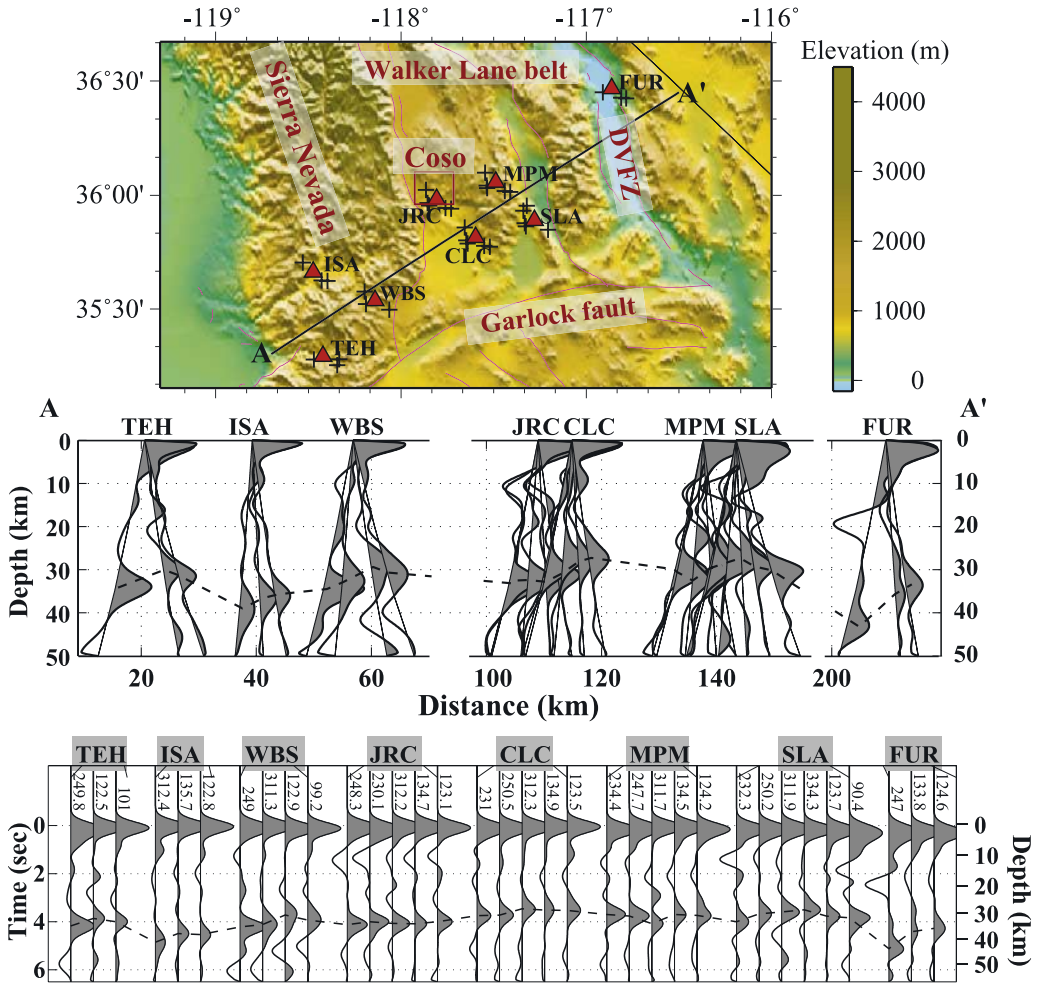

Figure 7. (top) Topography map of the Southern Sierra and nearby Walker Lane belt. Stations are marked by the red triangles with labels. Black crosses are the surface projections of the Pms conversion points at 30 km. DVFZ, Death Valley fault zone; TEH, the Tehachapi Mountain station. (middle) RFs projected onto line AA′. Some distance breaks are inserted in order to expand the RFs. (bottom) RFs evenly spaced but grouped by stations and sorted according to distance from point A. The averaged back azimuth for each group is labeled on the corresponding stacked trace. The dashed line on both plots represents the Moho P-to-S converted phase. The marked depth on both profiles is pseudodepth obtained by migrating the Ps-P time using the standard iasp91 model. The pseudodepth could be slightly different from the best estimated Moho depth from the grid search algorithm since different velocity models are used. In the following RF profiles, RFs will be presented either back-projected (as Figure 7, middle) or evenly spaced (as Figure 7, bottom) depending on the gaps between stations.

Lane belt. A deep Moho of 35–39 km beneath the western Sierra and its transition to a shallow Moho of 28–31 km to the east and south beneath the eastern Sierra, the Coso geothermal area, and the Tehachapi Mountains are imaged (Figure 6). A slightly deeper Moho of 32–35 km is observed in the eastern Sierra north of latitude 36.5°. The transition from deep to shallow Moho in the southern Sierra is relatively sharp and is evident from the RFs of the two neighboring stations ISA and WBS (Figure 7). More than 0.5 s Pms arrival time difference is observed between these two stations. Local deep Moho of 36–39 km is observed at several station groups in the Walker Lane belt. One example is station FUR at Furnace Creek in Death Valley. Pms arrives at ∼5.0 s for the southwest (SW) group of this station, and Moho depth is inferred to be 40 km, with a Vp/Vs ratio (κ) of 1.775 (Figure 8). A RF profile constructed from nearby station groups in the southern Sierra and Walker Lane belt is shown in Figure 7. It is clear that larger Pms arrival times and thus deeper Moho are observed at both ends (except TEH), while smaller Pms arrival times and shallower Moho are observed in the center beneath the Coso geothermal area. Midcrustal interface is generally absent in the RFs for most station groups, with the only exception being a prominent negative pulse at the SW back-azimuthal group of station FUR. This prominent negative pulse is consistently observed for all the RFs from SW at FUR, and the H–κ domain grid search indicates that it is at a depth of ∼20.5 km and the average κ is ∼1.73 (Figure 8). A similar

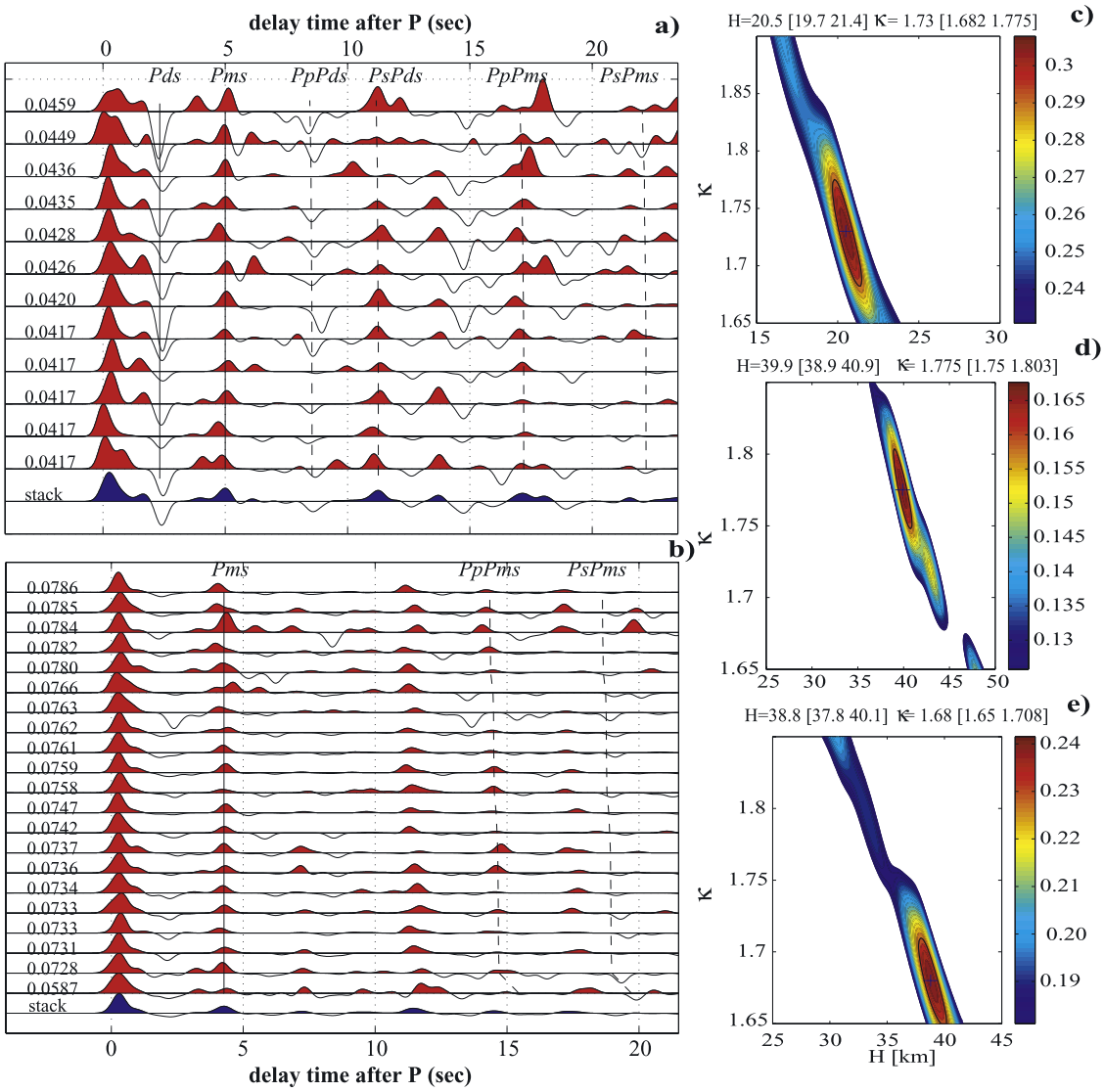

Figure 8. RFs for station FUR. (a) Representative RF traces for the SW back-azimuthal group. (b) RFs for the SE group. Picked arrival times for the primary phases and the corresponding multiples are marked by the dashed lines. (c and d) H-κ domain grid search contour for the midcrustal negative pulse (Pds) and Moho interface (Pms) for the SW group. (e) H-κ domain grid search contour of the Moho interface (Pms) for the SE group.

bright spot (velocity decrease interface) was imaged at ~20 km in the southern Death Valley by previous COCORP reflection studies [*de Voogd et al.*, 1986, 1988].

[15] Large differences in the Pms arrival time are observed among the different back-azimuthal groups at station FUR (Figure 7). As mentioned above, a late Pms arrival of ~5.0 s is observed for the SW group, but for the SE group, Pms arrives at ~4.5 s. However, a similar Moho depth of 38.8 with a slightly lower Vp/Vs ratio of 1.68 is inferred for this group (Figure 8). H and κ are relatively well constrained for the SE group because multiples are well developed. RFs for the SW group are slightly more noisy, but consistently high-amplitude Pms phase is observed in all the traces and the coincidence of the imaged velocity decrease interface (bright spot) with previous studies confirm the quality of the RFs for this group. Thus RF results for both groups seem to be reliable and a local deep Moho is inferred. The 0.1 difference in the Vp/Vs ratio between these two groups might be the result of the juxtaposition of different rock types along the Death Valley fault zone or might be related to complications in the Moho geometry. Another issue for the RFs at station FUR is that it is generally believed that thick low-velocity sediments exist in the Death Valley extended terrane [*Blakely et al.*, 1999], which can complicate the RFs. This does not seem to be the case at FUR, since no large-amplitude reverberations exist in the data.

[16] The imaged deep Moho beneath the western Sierra Nevada and its transition to the shallow Moho to the east are similar to the RF studies by *Jones and Phinney* [1998] and the traveltime tomography studies by *Fliedner et al.* [2000]. The local deep Moho beneath the Death Valley is similar to the result of previous traveltime tomography studies (~35 km on line P3) by *Fliedner et al.* [2000], but is very different from the shallow and flat Moho at ~30 km from early COCORP

reflection studies [*Allmendinger et al.*, 1983, 1987; *Hauge et al.*, 1987; *Hauser et al.*, 1987]. One reason for the difference may be that the Moho is below the illumination zone of the early reflection studies. Thus it is possible that a local deep Moho of 36–39 km does exist beneath the Death Valley, where large surficial extension was observed. This indicates that the upper crust is probably weakly coupled or decoupled from the lower crust in this region. The source of the 0.1 difference in the Vp/Vs ratio between the two back-azimuthal groups for station FUR is not known.

3.2. Peninsula Range and the Salton Sea

[17] In the Peninsula Range, Moho depth is generally around 32–34 km in the west. A sliver of thick crust of 34–38 km is observed in the southwest and it transitions to a shallow Moho of 20–25 km to the east close to the Salton Trough within a lateral distance of less than 50 km (Figure 6). Stations in Peninsula Ranges are divided into three groups separated by the major faults and RFs for them are shown in Figure 9, as well as for stations to the east of the Salton Trough. Shallowing of the Moho from west to east toward the Salton Trough is observed on all three profiles. A relatively shallow Moho of 32–34 km is commonly observed at the western stations of the two northern groups, as well as the westernmost three stations (BCC, CAP, GOR) of the southern group. A relatively deep Moho of 34–39 km is observed at several stations (PLM, DPP, EML, SDR, and BAR) in the center of the southern group. Large Pms arrival time differences are observed among the different back-azimuthal groups at stations WMC in the northern block, and SWS in the central block. Both stations are located close to the San Jacinto fault zone and thus depth extension of the San Jacinto Fault to the Moho is inferred. The Moho deepens very gradually to the east of the Salton Trough and reaches a depth of 25–28 km at ~100 km away beneath stations IRM and BLY. Asymmetric extension of the Salton Trough is thus inferred from the Moho depth variation pattern: Moho deepens sharply to the west beneath the Peninsula Ranges but very gradually to the east in the Mojave Desert.

[18] The observed Moho depth variation pattern in the Peninsula Ranges is similar to studies by *Lewis et al.* [2000, 2001] and *Ichinose et al.* [1996], but more details are presented here, in particular, shallowing of the Moho to the west of their profile to 32–34 km along the coast is inferred from stations CAP, BCC, and GOR, and asymmetric extension of the Salton Trough is inferred from comparison of the Moho depth variation for stations to the west of the Salton Trough with those to the east.

[19] The relatively sharpness in the deepening of the Moho depth from the Salton Trough to the Peninsula Ranges and the fact that thick crust of more than 30 km exists beneath the western Peninsula Ranges (WPR), which was transferred to the Pacific oceanic plate during the formation of the San Andreas strike-slip system, indicate that the crust beneath the WPR is of continental origin and that the W-NW movement of this block along the stable North American plate involves the whole crust. Strong coupling is thus inferred between the upper and the lower crust for the Peninsula Ranges block.

3.3. Mojave Desert and the San Bernardino Mountains

[20] For the Mojave Desert, a relatively flat Moho of 28–32 km is observed in the west, and a slightly shallower Moho of 26–28 km is found for most station groups in the east across the southern extension of the Death Valley fault zone, where the shallowest Moho of ~23–25 km within this region is inferred. A deep Moho of 34–39 km is observed beneath the San Bernardino Mountains. RFs profiles along three W-E lines, a N-S one from the nearby SCSN station groups, and one N-S profile from the LARSE I passive stations are shown in Figures 10 and 11.

[21] Along the northern W-E profile AA′ (Figure 10), Moho is flat beneath stations LRL and CCC at a depth of 29–31 km, shallows slightly beneath stations GSC and BKR, and reaches its minimum value of 23–25 km beneath the east back-azimuthal groups of BKR and DSC. The Moho then deepens and becomes more complicated farther to the east beneath station LDF. For this station, a mid-crustal negative pulse (velocity decrease interface) occurs at ~1.5 s (10–12 km), as well as an additional positive pulse at ~20 km. Another complication is the large difference in the Pms arrival time between the western and southeast (SE) back-azimuthal groups. Since no well-developed multiples exist for the two SE groups, sources for the difference in the Pms arrival time are unknown.

[22] For the central line, Pms has a relatively constant arrival time of 3.7–3.8 s, corresponding to a Moho depth of 29–32 km, for most station groups except for stations RRX and DAN. At RRX, late Pms arrival time of 4.3–4.5 s for the two SW back-azimuthal groups and a large Pms arrival time difference of 0.5 s between these two groups and those of NW and SE are observed. Since large amplitude reverberations, which are the characteristic of low-velocity sedimentary cover, exist and the two multiple phases, PpPms and PsPms, are not distinguishable from the reverberations, it is possible that the observed late Pms phase is not resulted from the true deepening of the Moho but from complications from the low-velocity sedimentary cover. The apparent delay of the direct P wave in the radial RFs also indicates the existence of low-velocity sediments beneath this station. Similar anomalous RFs are observed at another LARSE I station and will be discussed later. At station DAN, large Pms arrival time difference of ~1 s is observed between the NW and the SE back-azimuthal groups. For events from NW, Pms has an early arrival time of ~3 s, corresponding to a Moho depth of ~20.5–22.5 km. The late Pms at ~4.2 s for the SE group indicates a Moho depth of ~30.5–33.5 km. A Moho offset of ~8–10 km is thus inferred across the Moho conversion points of these two back-azimuthal groups, which are less than 15 km apart. Clear and distinguishable multiples are observed for both groups, and well-constrained Vp/Vs ratios of 1.845 and 1.805 are determined, respectively. The existence of clear multiples and the closeness of the Vp/Vs ratio for the two groups indicate that the imaged Moho step beneath this station is real and that the Moho is relatively smooth to either side of the station.

[23] For the southern W-E line, the Moho is essentially flat and shallows slightly to the east beneath stations MCT and IRM. A very prominent midcrustal interface is observed at the westernmost station ALP, which is similar to the midcrustal interface along the LARSE I line (discussed later).

[24] A deep Moho of 34–39 km is observed beneath the San Bernardino Mountains along the N-S SCSN profile and

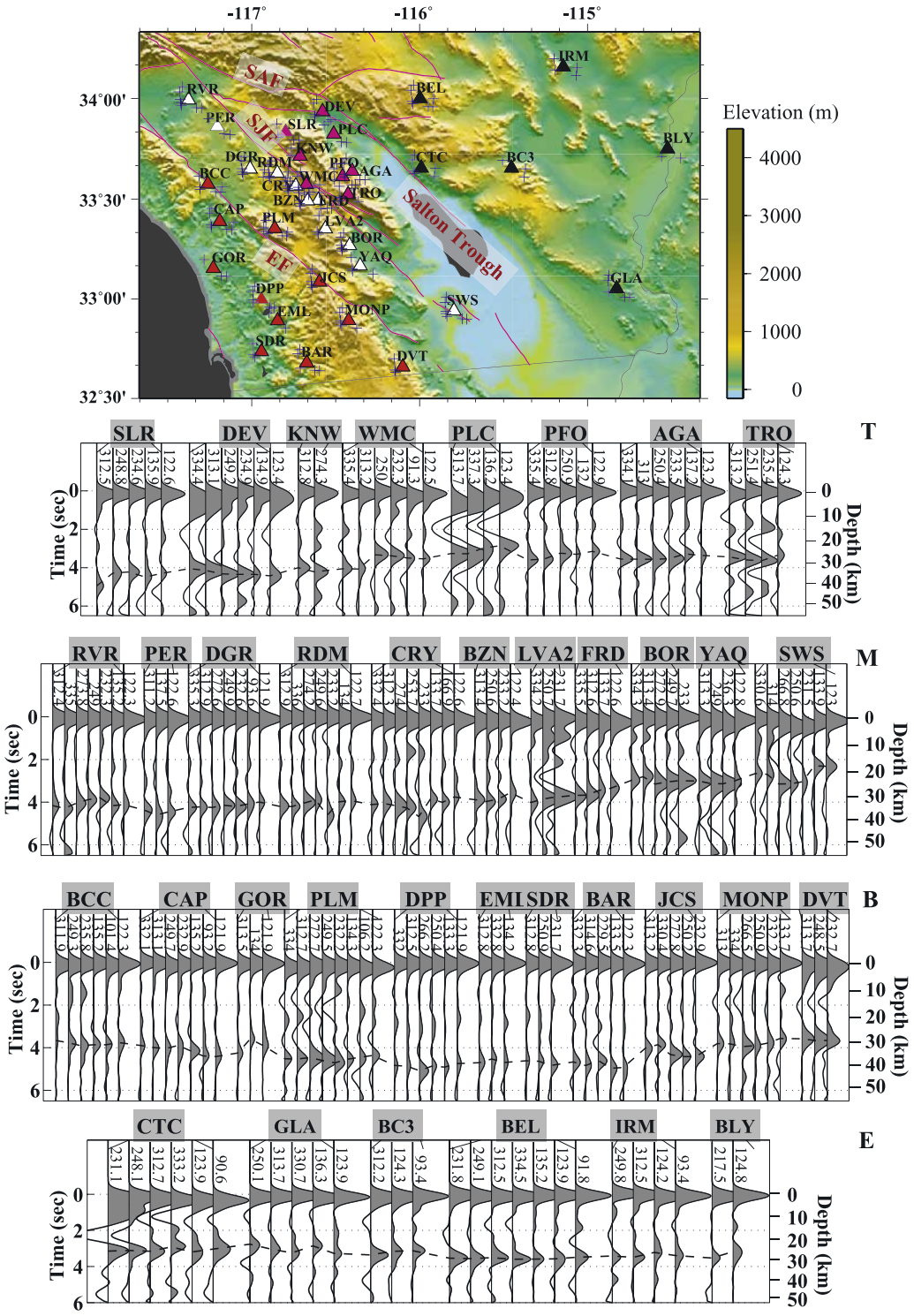

Figure 9. Similar to Figure 7. (top) Topographic map of the Peninsula Ranges along with stations and the piercing points. Stations are divided into four groups (different colors) separated by the major faults. SAF, San Andreas Fault; SJF, San Jacinto Fault; EF, Elsinore Fault. RFs for the four group are shown below. (bottom) Top group (T, purple stations), middle (M, white), bottom (B, red), and east (E, black) station groups. Similar to Figure 7 (bottom), the traces are evenly spaced but grouped by stations.

its NW extension on the LARSE I profile (Figure 11). For the SCSN station profile (DD′), two sets of flat/ramp/flat Moho depth variation patterns are observed. The southern step is related to the shallowing of the Moho from ~34–39 km beneath stations SVD and BBR in the San Bernardino Mountains to ~29–31 km beneath stations JVA, NBS, and HEC in the western Mojave Desert. The second step correlates to the Moho shallowing from the western Mojave

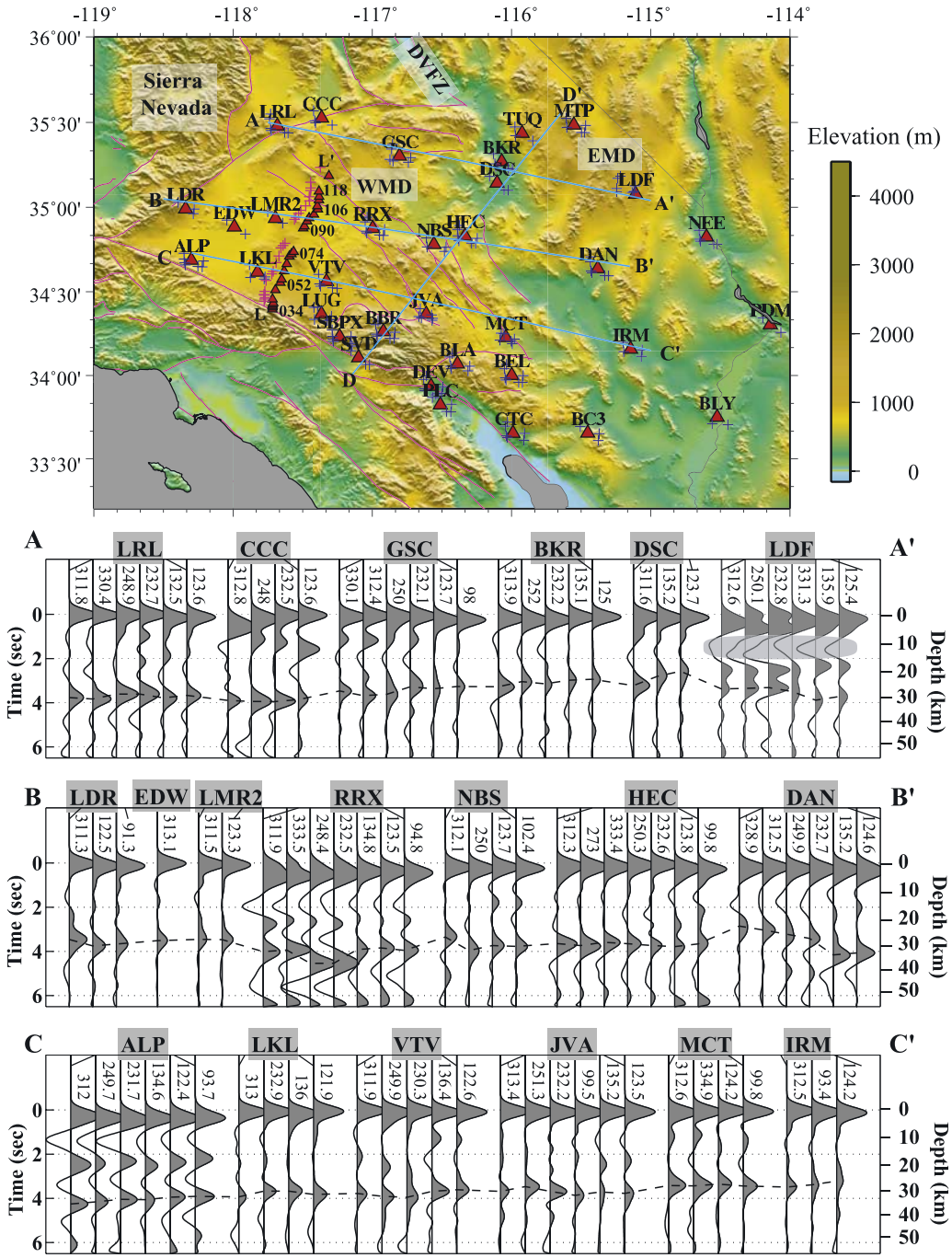

Figure 10. Similar to Figure 7. (top) Topographic map of the Mojave Desert along with stations and the piercing points. Large triangles are the SCSN stations, and blue crosses are the conversion points. Small red triangles and the pink crosses are for the LARSE I passive stations. The green lines are the four profiles along which the RFs of nearby station groups are shown in the following. WMD, Western Mojave Desert; EMD, Eastern Mojave Desert; DVFZ, Death Valley fault zone. (bottom) RFs along the three west-east profiles. Similar to Figure 7 (bottom), the RFs are evenly spaced but grouped by stations and sorted according to their distances from the western end points due to the large distance gap between stations. The light gray shaded negative pulse on the eastern end of profile AA′ is a velocity decrease interface.

Desert to the eastern Mojave Desert beneath stations BKR, TUQ, and MTP, where a slightly shallow Moho of ∼26–28 km is observed. Similar to profile AA′, the Moho reaches a minimum of 23–26 km beneath the SE station groups of DSC and BKR in the southern extension of the Death Valley fault zone. For the LARSE I profile, only the southern step related to the shallowing of the Moho from the NW extension of the San Bernardino Mountain root to the

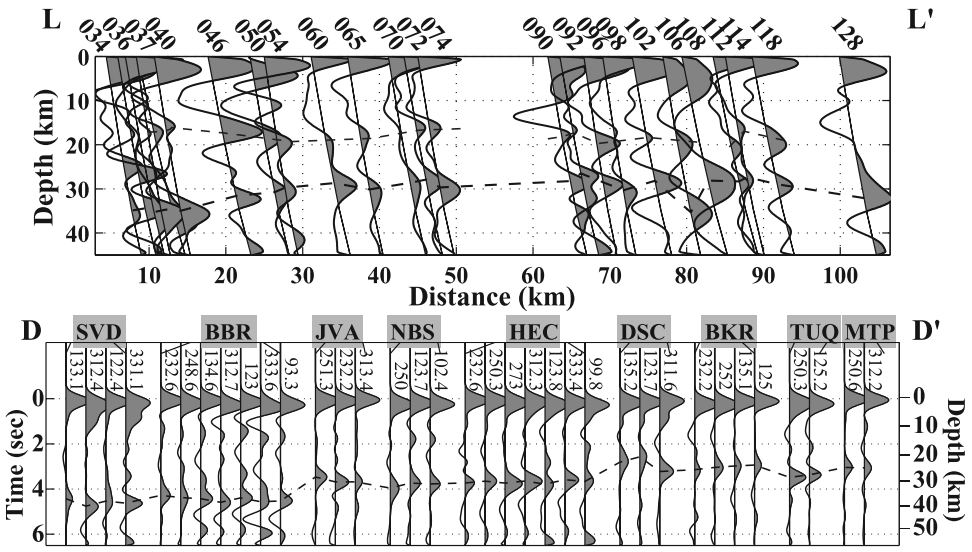

Figure 11. RFs profiles along the north-south oriented LARSE I and the SCSN profiles in Figure 10. (top) LARSE I RFs plotted according to their distance to the southern point L, as in Figure 7 (top). (bottom) RFs evenly spaced similar to Figure 7 (bottom).

western Mojave Desert is observed. A flat Moho at 29–31 km and a low-amplitude midcrustal interface at ~18–20 km is commonly observed for most LARSE I stations (from station 037 to the north). Exceptions to this pattern are observed at stations 106 and 108, which will be discussed in the following paragraph. The deep Moho imaged beneath the San Bernardino Mountains and the Mojave side of the LARSE I profile are most probably connected with each other at depth due to their proximity. This indicates that the deep root of the San Bernardino Mountains most probably extends farther to the NW, where no surficial topography high exists. A similar deep Moho is inferred by *Zhu* [2000] and *Kohler and Davis* [1997] from RF and teleseismic P traveltime studies, respectively.

[25] Unusual RFs are observed at LARSE I stations 106 and 108. A very late Pms arrival time of 4.3–4.5 s is observed at station 106, and its midcrustal Ps phase is also delayed comparing with other stations in the western Mojave Desert. The pattern is similar to the SCSN station RRX (Figure 10). No midcrustal interface is observed at station 108, and the Pms pulse is much wider than others. The unusual RFs at these three stations reflect local complications in the crustal structure beneath them. If the stations are mapped onto the two-dimensional kinematic model of *Dokka and Ross* [1995], they actually fall onto the transtensional zones (''gaps'') where deep openings developed between the rotated blocks [*Yan*, 2007]. Thus the late Pms at these stations may be due to the local complex structure instead of true Moho deepening.

[26] A dipping interface is known to generate systematic Pms variation with back azimuth [*Peng and Humphreys*, 1997; *Cassidy*, 1992]; in particular, significant Pms arrival time difference is observed between the updip and the downdip directions. The observed large Pms arrival difference at station DAN (Figure 10), however, does not seem to be caused by a dipping Moho. First, the arrival time and amplitude variation pattern of the Pms phase on the radial component does not conform to a dipping interface. In theory, RFs from the updip direction have both a small-amplitude Pms phase and an early Pms arrival time. The data, however, do not show such patterns since large Pms phase is observed for the NW direction, which is supposed to be the updip direction from arrival times. Secondly, the difference in the Pms arrival time (~1 s) is too large for it to be caused by a smooth dipping interface at around 30 km (the time difference for a 20° dipping layer at 60 km is around 1 s [*Cassidy*, 1992]). Furthermore, the shallow Moho to the west side of this station is confirmed by the SmS-S traveltime difference studies from the Hector Mine aftershock sequences by V. Hjorleifsdottir and D. Helmberger (Velocity variations in the lower crust beneath the Mojave Desert, personal communication, 2001).

[27] The shallow Moho in the eastern Mojave desert was previously imaged by several studies [*Zhu and Kanamori*, 2000; *Richards-Dinger and Shearer*, 1997; *Hearn and Clayton*, 1986b], but more details about the localized anomalies are presented here. The large difference in the Pms arrival times among the different back-azimuthal groups for stations LDF and DAN, as well as the complications in the RFs for station LDF itself, indicate that the crustal structure in the eastern Mojave Desert is more complicated than that to the west. Another indication of the complications in the eastern Mojave Desert is the existence of a prominent negative pulse just below Moho at the SE groups of DAN (BB′ in Figure 10). This could be the upper boundary of a magma chamber or it might indicate that the upper mantle lithosphere is thin in this area, similar to the thin warm lithosphere observed beneath the eastern Sierra [*Wang et al.*, 2002]. Extensive Quaternary volcanic activity is observed in the eastern Mojave Desert [*Jennings*, 1975; *Jennings and George*, 1994; *Kaufman and Royden*, 1994] but is absent in the west. All these indicate that the eastern Mojave Desert is tectonically very different from the western Mojave Desert [*Snow and Wernicke*, 2000]. The existence of a shallow Moho and extensive Quaternary volcanic activity in the eastern Mojave Desert also confirms previous observations that active extensional

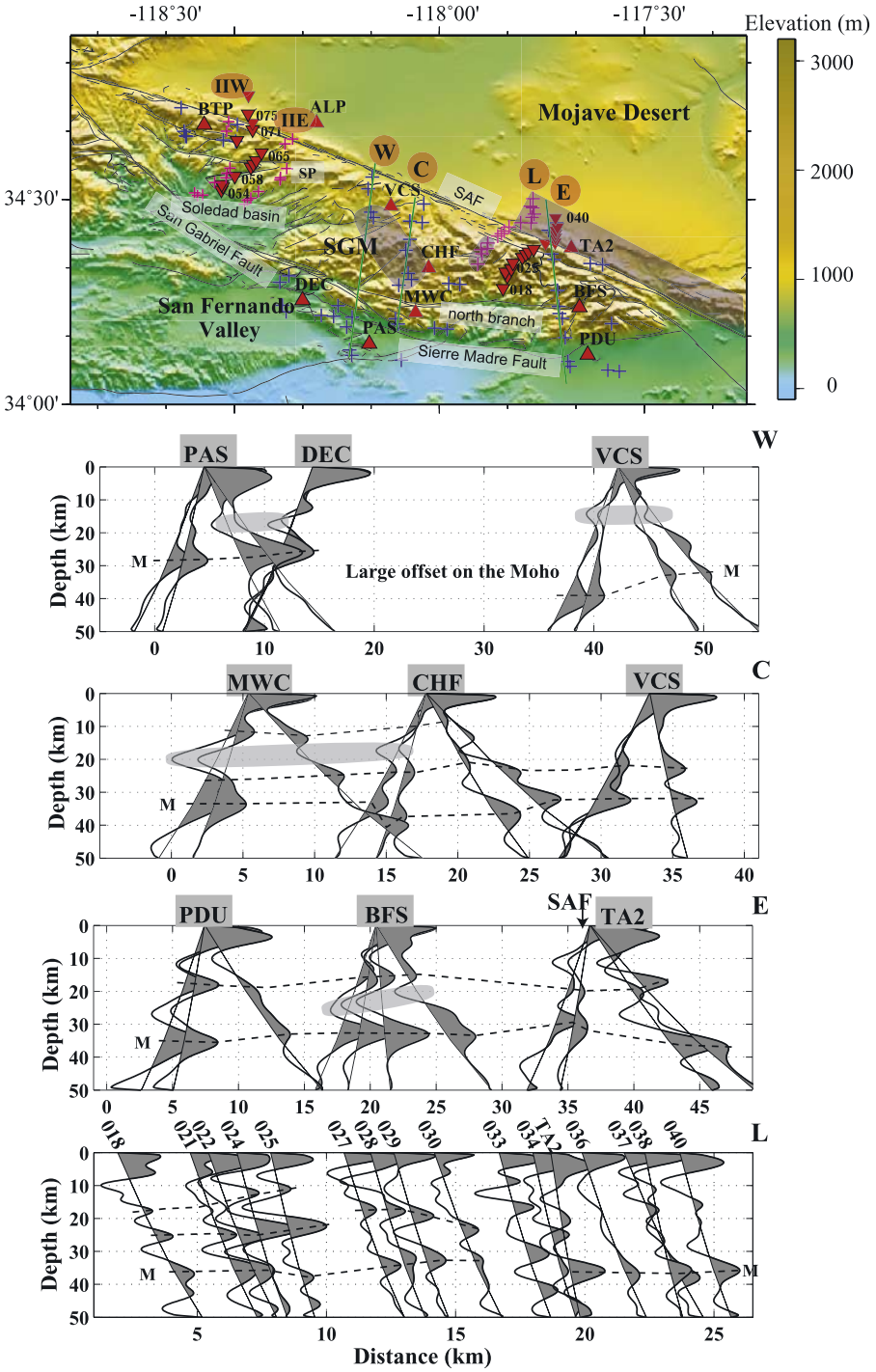

Figure 12. (top) Topographic map of the San Gabriel Mountains along with stations and the conversion points at 30 km. Labels are the same as those of Figure 7. Inverted triangles are the LARSE passive stations with representative stations labeled. The three green lines are the three SCSN profiles. SGM, San Gabriel Mountains; SAF, San Andreas Fault; SP, Sierra Pelona. The shaded areas on the map represent the local mountain roots where a deep Moho of 35–39 km is inferred. Station groups in the nonshaded area have relatively shallow Moho of 28–34 km. (bottom) RFs for the three south-north SCSN profiles and the LARSE I line (L). Similar to Figure 7 (top), RFs are projected along the corresponding lines. Moho Pms phase (M) and midcrustal Ps phases are marked by the dashed lines. On the profiles, the lightly shaded areas represent the bright spot.

zones normally correlate with thin crust and high geothermal activities [*Abers et al.*, 2002].

3.4. San Gabriel Mountains

[28] Most stations in the San Gabriel Mountains show large Pms arrival time variations with back azimuth. One example is station VCS shown in Figure 3. Pms has an early arrival time of 3.8–4.2 s for events from SE and NW, but has a late arrival time of 4.8 s for events from SW. No distinguishable multiples are observed for any back-azimuthal groups (such as the SW group shown in Figure 4). Multiples for other station groups in the western San Gabriel Mountains are also missing, and consequently none of the station groups are qualified for the Moho depth map in Figure 6. Since prominent Pms and some midcrustal phases are consistently observed at most station groups, three N-S cross sections were constructed from the SCSN stations, as well as three profiles from the LARSE surveys (Figures 12 and 13).

[29] Dramatic change in the Pms arrival time is observed between the northern and southern station groups (separated by the San Gabriel Fault) along the western profile (Figure 12). Pms has an early arrival time of 3.6–3.8 s for the southern station groups, corresponding to a shallow Moho at 27–29 km, but increases to ~4.8 s, corresponding to a Moho depth of ~38 km, beneath the SW station groups of VCS in the north. It then decreases back to ~4.0 s farther north beneath the NW groups of VCS. A midcrustal interface at about 23 km is observed at all back-azimuthal groups of VCS, which is absent in the southern station groups.

[30] The Moho also has some local variations along the central profile. A local deep Moho of ~34–38 km is observed at the NW station group of MWC and the SW and NWW station groups of CHF (distance range 12–25 km), and it shallows both to the north beneath the SE station groups of VCS and to the south beneath the SW station groups of MWC. Two midcrustal interfaces are imaged beneath most of the station groups for the two southern stations WMC and CHF. This corresponds to a three-layered crustal structure, and depths to the two midcrustal interfaces are 8–10 km and 22–25 km, respectively.

[31] Moho is relatively flat at 31–34 km on the southern portion of the eastern profile but gets complicated farther to the north. Large offset of 7–10 km is inferred between the NW and SW back-azimuthal groups of the northern station TA2: Deep Moho of 36–39 km is inferred for the NW station groups but shallows to ~28–30 km to the south across the San Andreas Fault for the two SW groups. One midcrustal interface at ~16–18 km is commonly observed along the eastern profile, which corresponds to a two-layered crustal structure, and is thus in contrast to the three-layered crustal structure on the central profile.

[32] Large lateral variations in the RFs are observed along the LARSE I profile. The southern station groups (018–022) generally have two midcrustal interfaces and show a deep Moho of 35–38 km. RFs for the two farther northern stations, 024 and 025, have a very large P-to-S converted phase at 2.7–3.0 s (corresponding to a depth of 24–26 km). Interpretation for the RFs of these two stations can be controversial. If Moho Pms is the phase that has the largest amplitude between 2.5 and 5.0 s, then the interface at 2.7–3.0 s should be the Moho Pms and thus a very shallow Moho of 24–26 km is inferred, as interpreted by *Zhu* [2000]. However, if continuity of the interfaces is assumed, then this large-amplitude interface seems to correlate very well with the 2.8–3.0 lower crustal interface for stations 018–021, and the later interface at ~4.8–5.0 s should be interpreted as the Moho Pms since it is very close in time to the picked Pms phase for the three southern stations. The amplitude of the Pms phase can be reduced by diffractions if lateral heterogeneity exists in the crustal structure. *Zhu* [2002] found significant amplitude contrast for the Pms phase across the San Andreas Fault, with low-amplitude Pms phase imaged beneath the central Transverse Ranges. So, the deeper low-amplitude interface on 024–025 is a candidate for the Moho. For the four farther northern stations (027–030), Moho is relatively flat at a depth of 31–34 km, similar to the southern station groups on the eastern profile. Multiple reverberations are observed for the two stations on the San Andreas Fault (033–034), and no prominent Pms phase is observed. Farther to the north across the San Andreas Fault, a deep Moho of 36–39 km is found for the four stations (036–040) as well as the SW group of station TA2.

[33] RFs along the LARSE I profile are generally consistent with those along the SCSN profiles. Furthermore, the transition from the three-layered crustal structure typical of the central profile to two-layered structure commonly observed on the eastern profile is clearly imaged on the LARSE I profile from the lateral variations of the RFs from station groups 018–022 to 027–029. The deep Moho to the north of the San Andreas Fault (036–040) also conforms to the result of SCSN station TA2.

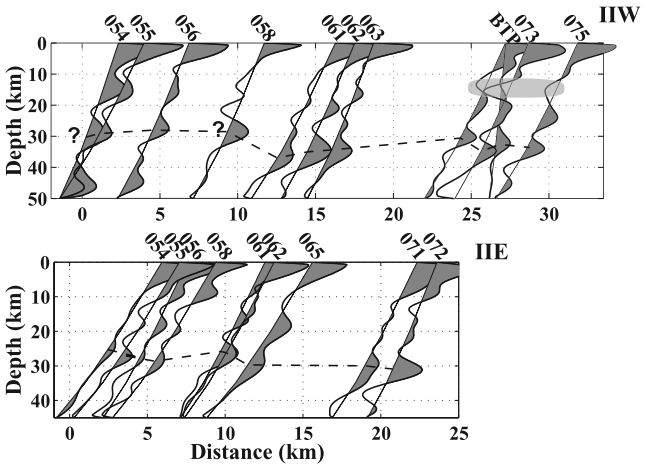

Figure 13. RF profiles along the SW and the SE back-azimuthal groups of the LARSE II line. Similar to Figure 7 (top), RFs are projected onto two straight lines. Note the similarity of the RFs between the LARSE II SE station groups and the SCSN station BTP. They all show a three-layered structure. The SE groups sample the depth extension of the Sierra Pelona and shows a shallow Moho of 31–33 km. Also, note the difference in the RFs between station BTP here and station ALP in the Mojave Desert (Figure 10).

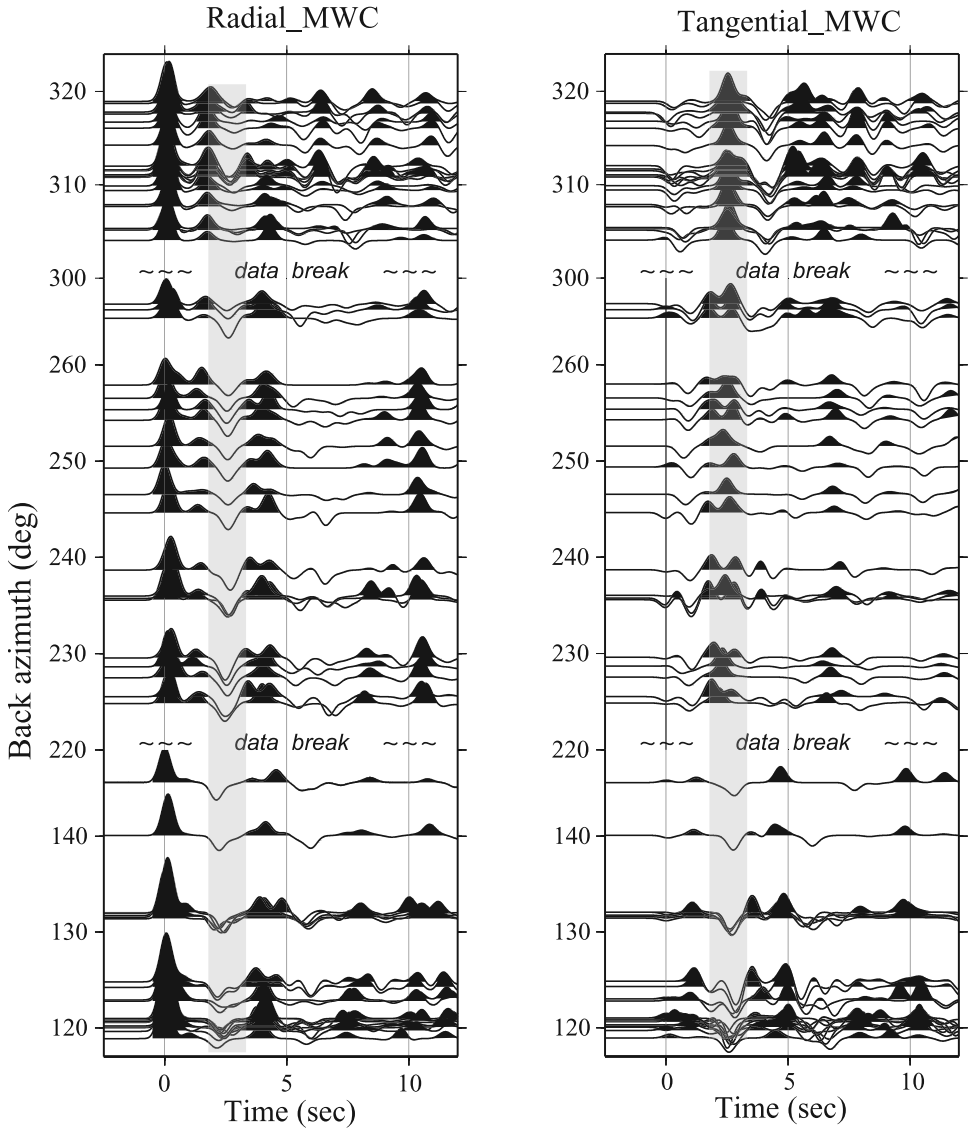

Figure 14. Radial and tangential RFs for station MWC (Mount Wilson) in the San Gabriel Mountains. Note the amplitude variation of the midcrustal interface at 1.8–2.0 s (shaded). The amplitude of this phase is largest for RFs at back azimuth [220, 230] on the radial component and diminishes for the SE group and is almost zero for the NW group. For the tangential component, the amplitude is higher for the NW and the SE back azimuths, but polarity is reversed, and amplitude is near zero for the back-azimuth range [225, 260]. The amplitude variation pattern of this phase on both components indicates that it is a SSW dipping interface. Because of poor back-azimuthal coverage, the exact dip direction is not very well constrained.

[34] The SW and SE back-azimuth groups for some of the LARSE II passive stations are shown in Figure 13, as well as the southeast groups of the SCSN station BTP. Moho depth is generally at 31–35 km for the SW group and 28–31 km for the SE group. Complications in the RFs for the four southernmost stations on the SW profile are probably due to the influence from the low-velocity sediments in the nearby Soledad basin (Figure 12). A three-layered crustal structure is inferred for most station groups along both profiles and a prominent negative pulse is observed at stations 073 and 075 on the SW profile, as well as the SE group of station BTP. The depth to this negative pulse is ~15 km, which is slightly shallower than that on stations to the east in the San Gabriel Mountains.

[35] A midcrustal negative pulse, which corresponds to a velocity decrease interface, is commonly observed on all three SCSN profiles (Figure 12) in the San Gabriel Mountains. The arrival time of it varies from 1.9 to 3.0 s, corresponding to a depth of 15 km to 24 km. It is also imaged in the SE groups of station BTP and the SW groups of two LARSE II stations, 073 and 075 at a slightly smaller time (see Figure 13). Thus the "bright spot" seems to be a common feature beneath the Central Transverse Ranges. It is very well developed at stations MWC and CHF in the western San Gabriel Mountains. Amplitude variations of this interface on the radial and tangential components of station MWC (Figure 14) indicates that it dips to the S-SSW. Because of limited back-azimuthal coverage of the

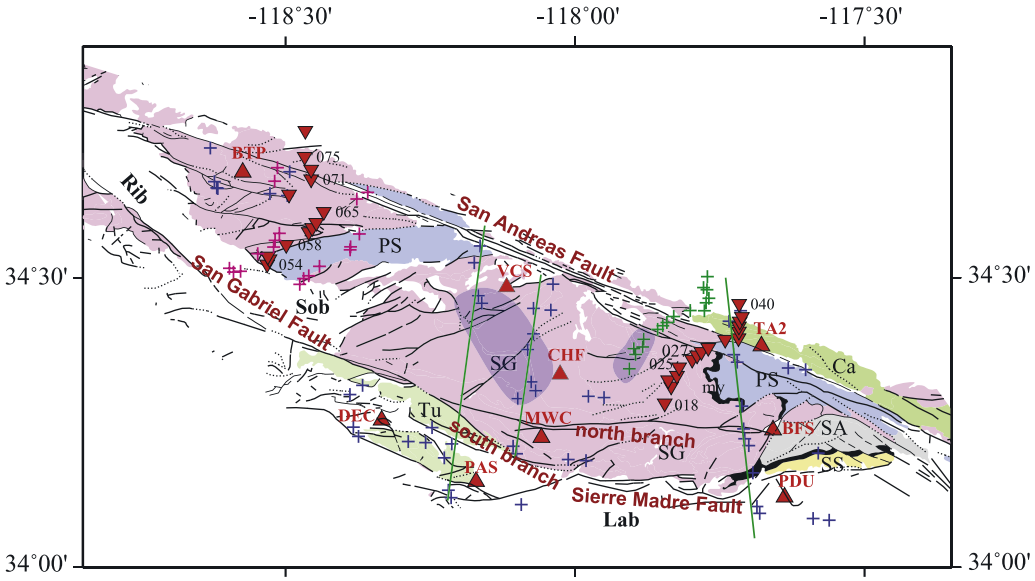

Figure 15. Revised geological terrane map of the San Gabriel Mountains [*Dibblee*, 1982b], with stations and the conversion points at 30 km marked. Colors represent the different terranes, and symbols are the same as those in Figure 12. The bold black characters are basement terrane names. SG, San Gabriel terrane; SA, San Antonio terrane; SS, San Sevaine terrane; Tu, Tujunga terrane; my, mylonite; PS, Pelona Schist terrane; Ca, Cajon terrane. Cenozoic sedimentary basins are also marked. Lab, Los Angeles basin; Sob Soledad basin; Rib, Ridge basin. Shaded areas are the local deep Moho imaged from this study.

data, the exact dipping direction is not resolvable here. This "bright spot" was previously identified by *Ryberg and Fuis* [1998] along the LARSE I reflection profile; they proposed that it was caused by fluids. Three reflectors were imaged at the top of the bright reflective zone, and they were interpreted to be gently north dipping on the basis of the clear north dip on the northern portion of the interface. However, a gentle south dip of the interface is clear from their image for the southern portion of the interface [*Ryberg and Fuis*, 1998] and thus is in agreement with this study. This means that the bright spot is probably not a simple planar interface, but forms a dome shape, as indicated by the reflection image [*Ryberg and Fuis*, 1998]. No prominent negative pulse is observed on the LARSE I RF profile (Figure 12) probably due to the fact that the events for the LARSE I profile are from the updip (NW) direction of the interface and thus have negligible amplitudes [*Savage*, 1998].

[36] The bright spot (the negative pulse) is interpreted as accumulated fluid along a "master" decollement that separates the lower plate Pelona Schist from lower continental crustal rocks. They also imaged a positive polarity event for shot 8330 along the LARSE I profile 0.2 sec later than the bright reflector and thus constrain the thickness of the low-velocity layer to be around 500 m. An approximate estimate on the thickness of this layer can be made from this study if the positive phase just below the negative one along the central SCSN profile (Figure 12) is the bottom of the low velocity layer: The thickness for it is then constrained to be ~2–4 km.

[37] By observing the available RFs for stations in the San Gabriel Mountains, one common conclusion can be drawn: The crustal structure beneath this mountain range is strongly laterally heterogeneous. Evidence includes (1) large difference in the Pms arrival time among the different back-azimuthal groups for individual stations (such as VCS, TA2, and CHF); (2) the absence of well-developed multiples for most station groups; (3) the large difference in the crustal structure between the eastern and the central profile, two-layered crustal structure on the eastern profile but three-layered along the central one; and (4) large lateral variations of the RFs along the LARSE I and the western SCSN profiles (Figure 12). Another indication of the complications is the lack of consistent Pms phase for some station groups and the systematic variations of the RFs with ray parameter. An example for the latter is the W-NW group of station BFS, where single large amplitude Pms phase is observed for RFs at small ray parameters, but double smaller-amplitude phases are evident at larger ray parameters ($\geq$0.065). This is explained by the existence of a notch structure on the Moho [*Yan*, 2007].

[38] Complications in the subsurface structure beneath the San Gabriel Mountains correlate well with the surficial geology of the basement terrane map [*Dibblee*, 1982b] (Figure 15). One example is the large difference in the RFs between the northern and the southern station groups along the western profile. All the southern station groups that share a shallow Moho are mapped onto the Tujunga terrane, while the SW groups of VCS, which has a deep Moho, fall onto the San Gabriel terrane. The two terranes were juxtaposed together by the ~60 km strike-slip movement along the San Gabriel Fault. The difference in the RFs between the NW and the SW groups of VCS can also be explained by the proximity of the NW group to the lower plate Pelona Schist terrane. Stations on the eastern and the central profiles are also mapped onto different terranes: All the stations on the central profile are on the San Gabriel

terrane, while the three stations on the eastern profile are mapped onto three different terranes. The various terranes are proposed to have distinctive tectonic evolution histories and were juxtaposed together from distant locations [*Ehlig*, 1981; *Dibblee*, 1982a]. The large-scale correlation between the subsurface structure and the surficial terrane distribution indicates that strong coupling probably exists between the upper and lower crust beneath the San Gabriel Mountains and that the current subsurface structure have retained large amount of their prejuxtaposition features.

3.5. Tectonic Implications

[39] There are some controversial results as to whether the San Gabriel Mountains have a root. *Kohler and Davis* [1997] inferred the existence of a deep root of 40 km centered at the San Andreas Fault from teleseismic P arrival time residuals along the LARSE I line. For the same data set, *Zhu* [2000] used teleseismic RF studies and imaged a shallow Moho of 25–31 km on the San Gabriel side, and a deep Moho of 37–40 km on the Mojave side along the LARSE I line. Results from this study indicate that large lateral variations exist in the crustal structure beneath the San Gabriel Mountains and that the Moho reaches a depth of 35–39 km locally beneath several station groups in the western San Gabriel Mountains. The approximate location of the inferred deep Moho is marked in Figure 12. No regional deep Moho exists beneath the San Gabriel Mountains, especially beneath the highest eastern San Gabriel Mountains, where an intermediate Moho depth of 32–34 km is inferred. Various factors along the raypaths may contribute to the observed teleseismic P traveltime delay patterns by *Kohler and Davis* [1997], and the method itself suffers from the trade-off between the crustal thickness and the crustal velocities. The absence of a regional root is also consistent with the observed positive Bouguer gravity anomaly in this area [*Langenheim*, 1999; *Wooley and Langenheim*, 2001]. The dominant existence of a shallow Moho beneath most station groups in the San Gabriel Mountains indicates that the crust of the SGM is not regionally thickened as inferred by *Kohler and Davis* [1997] and thus it is most probably not involved in the downwelling of the subcrustal lithosphere. Thus the results of this study support the decoupling kinematic model of *Humphreys and Hager* [1990].

[40] This study confirms the results of previous study [*Zhu*, 2000] which suggest that the San Andreas Fault (SAF) extends to the Moho and cuts through the whole crust. A deeper Moho of ~35–40 km and a shallower Moho of ~29–32 km are inferred for the Mojave side and the San Gabriel side of the SAF, respectively. More evidence of the depth extension of the SAF to the Moho can be drawn from the difference in the RFs between station ALP and BTP. The two stations are ~25 km apart, separated by the SAF (Figure 12). For station BTP (Figure 14), two midcrustal interfaces exist at depths 10–12 km and ~20 km, and Moho is relatively shallow at ~31 km. For station ALP (Figure 10), only one large-amplitude midcrustal interface exists and Moho is at ~34 km. Hence the crustal structure on the two sides of the SAF is quite different and the depth extension of the SAF to the Moho is suggested. Similar situation is observed for several other major faults, such as the San Gabriel Fault. The large difference in the RFs between the southern and the northern station groups on the western profile, as well as the southern groups on the western profile with those on the central profile, indicates that the San Gabriel Fault also cuts through the whole crust. Large offsets on the Moho are also observed beneath some individual stations where no surficial major faults exist. One example is at station DAN in the eastern Mojave Desert (Figure 10). A large Moho offset of 8–10 km is inferred between the NW and the SE groups of this station even though no surficial major fault exists here. Discontinuities in the lower crust can also be inferred from the RF data, such as the transition from the two-layered structure on the eastern profile to three-layered on the central profile in the SGM (Figure 12), and the abrupt appearance of an additional lower crustal interface at ~20 km beneath station LDF in the eastern Mojave Desert (Figure 10). All these large discontinuities in the lower crust and Moho depth indicate that either the lower crust or the upper mantle is sufficiently strong to resist the shear stresses induced by the difference in the lithostatic stresses from the above rock columns and that the Moho is more actively involved in the dynamics of the lithosphere than a passive smooth interface.

3.6. Uncertainty Consideration

[41] On the regional Moho depth map of Figure 6, uncertainty in the Moho depth from the grid search algorithm is shown, which is generally less than 2 km. Another source of uncertainty is from the average crustal P velocity. For consistency, it is assumed to be 6.3 km/s for all station groups. However, from studies of *Hadley* [1978], *Hearn and Clayton* [1986a, 1986b], *Hauksson and Haase* [1997], *Hauksson* [2000], and *Godfrey et al.* [2002], Pg velocity varies from ~6.2 km/s beneath the Sierra Nevada to ~6.5 km/s beneath the San Gabriel Mountains and the western Peninsula Ranges. Hence the true average crustal P velocity for different stations may deviate from the assumed 6.3 km/s by ±0.2 km/s. This deviation in the average crustal Vp might add an additional ±1.0 km in the Moho depth estimates. Another issue is the influence of the low-velocity sedimentary cover on the average crustal velocity and its offset on the Moho depth estimates. For stations in deep sedimentary basins, especially those with complicated geometries (such as stations in the Los Angeles basin), the calculated RFs normally have low signal-to-noise ratio and multiple basin reverberations, and are thus excluded from this study. For stations covered by thin sediments (less than 1 km), such as ALP (Figure 10), reasonable RFs are generated, but the first main pulse on the RFs is slightly shifted to the right due to the large amplitude of the primary P-to-S conversion from the high-velocity contrast sediment-basement interface and the closeness of the arrival time of this phase with the direct P. In this situation, the arrival time of the Pms phase is not influenced, but the determined Moho depth might be slightly overestimated due to the reduction of the average crustal Vp by the low-velocity sediments. Since the thickness of the sedimentary cover is thin, the reduction should be minor.

[42] One potential problem for all the profiles in this study is the lateral variations of the Vp/Vs ratio. Deviations of the Vp/Vs ratio from the standard iasp91 model can change the migrated depth for the RFs, which implies that some of the large lateral variations in the Pms arrival time could be the result of difference in the Vp/Vs ratio instead

of Moho depth. However, it is very unlikely for them to be attributed to the lateral variations in the Vp/Vs ratio alone, especially for those among the different back-azimuthal groups of the same station (such as at station DAN), since all the profiles are constrained to a localized region and rays from different directions converge at shallower depths ($\leq$10 km). Thus the inferred Moho offset among the different back-azimuthal groups at a particular station is unlikely to be an artifact from lateral variations in the Vp/Vs ratio. In fact, previous studies in the San Gabriel Mountains and the Mojave Desert indicate that the different rock types, except the San Gabriel anorthosite complex, all have a Vp/Vs ratio that lie within a limited range of 1.67–1.756 at greater depths ($\geq$10 km) (converted from the Poisson's ratio of *Pellerin and Christensen* [1998]). The variation range of the Vp/Vs ratio is not significant enough to explain the large difference in the Pms arrival time observed by this study.

4. Conclusions

[43] High resolution lateral variations of the crustal structure in southern California are obtained from back-azimuthal grouped receiver functions of both the SCSN stations and the LARSE passive stations. Distinctive features in the subsurface crustal structure are identified for individual regions. Large lateral variations in the crustal structure are imaged both beneath individual stations and across the major faults. The lateral variations are especially prominent in the San Gabriel Mountains, the eastern Mojave Desert, across the San Andreas Fault, the San Gabriel Fault, and the San Jacinto Fault.

[44] Large lateral variations in the crustal structure beneath the San Gabriel Mountains (SGM) are suggested by several types of evidence: (1) the large difference in the RF waveform for the nearby station groups, such as those along the western SCSN profile and the LARSE I profile; (2) lack of well-developed multiples for most station groups in the western San Gabriel Mountains; and (3) lack of a consistent Pms primary phase for some station groups. The strong correlation between the lateral variations of the RFs and the surficial basement terrane distributions indicates that strong coupling exists between the upper and the lower crust in this area, and that the current crustal structure (including Moho depth) retained some of its original individual terrane features before the juxtaposition. The absence of a deep Moho for a large portion of the station groups indicates that the crust was not regionally thickened as predicted by the strong coupling model and the crust of the SGM is probably decoupled from the sublithospheric "drip" structure on a 20–30 km scale. This study also indicates a wide spatial distribution of the bright spot beneath the San Gabriel Mountains with a local dip direction of S-SSW in the southern portion of the western San Gabriel Mountains.

[45] RFs in the western Mojave Desert are generally simple and do not show significant variations with back azimuth, which imply a relatively simple and smooth Moho. The absence of midcrustal interfaces in most SCSN stations in this region and a relatively low-amplitude midcrustal interface along the LARSE I profile indicate that the crustal structure here is very different from that beneath the San Gabriel Mountains. The Moho depth is generally around 29–31 km here. A shallower Moho of 23–26 km is observed beneath the topography low of the southern extension of the Death Valley fault zone (DVFZ), where active extension is dominant. The crustal structure becomes complicated to the east across the DVFZ in the eastern Mojave Desert, especially beneath stations LDF and DAN, where a Moho step of 8–10 km is inferred between the NW and the SW back-azimuthal groups of DAN. The appearance of a midcrustal negative pulse at 12–15 km and a following positive one at $\sim$20 km beneath station LDF indicates that the crustal structure is laterally heterogeneous across the DVFZ. A deep Moho of 35–39 km is inferred beneath the San Bernardino Mountains and its NW extension along the San Andreas Fault.

[46] A deep Moho of 35–39 km is observed along a sliver in the western Peninsula Ranges and it changes sharply to a shallow Moho of 19–22 km to the east near the Salton Trough. Moho deepens very gradually to the east of the Salton Trough, and thus asymmetric extension of the Salton Trough is inferred. Since the Peninsula Ranges block was transferred to the Pacific plate during the formation of the current San Andreas fault system at $\sim$5 Ma, the deep Moho here indicates that the crust of the western Peninsula Ranges is of continental origin and that the W-NW movement of it along the stable North American plate has involved the whole crust.

[47] Large lateral variations in the crustal structure are also observed beneath the Sierra Nevada and the nearby Walker Lane belt. A deep Moho of 36–39 km is observed in the western Sierra Nevada and two station groups in the northern Walker Lane belt. Flat shallow Moho of 28–31 km is observed beneath the Coso geothermal area and the southernmost Walker Lane belt. Existence of a deep Moho beneath the Death Valley fault zone, where the upper crust is highly extended, indicates that the upper crust was probably weakly coupled or decoupled from the lower crust during the Cenozoic deformation and that the Moho is probably not as flat as previously believed beneath the Basin and Range.

[48] Large-scale Moho depth variations generally correlate well the current state of the Mesozoic batholith: Deep Moho of 36–39 km is observed beneath the relatively intact Sierra Nevada, the western Peninsula Ranges, and the San Bernardino Mountains [*Jennings*, 1977], and shallow Moho of 28–31 km is observed beneath the highly deformed and attenuated Mojave Desert block and the Coso geothermal area. Geothermal activities also seem to have some correlation with the subsurface structure. The shallowest Moho in the study area are located in the highly extended Salton Trough and the topography low of the southern extension of the Death Valley fault zone in the Mojave Desert, where high heat flow and extensive Quaternary volcanic activities are observed. The general correlation between the upper crustal deformation and the subsurface crustal structure implies that the upper and the lower crust were generally coupled during the Cenozoic deformations. The only exception to this pattern is at station FUR, where a deep Moho of $\sim$36–39 km is observed in a surficially highly extended area. This means that decoupling of the upper and the lower crust may also exist in some areas.

[49] **Acknowledgments.** We thank the Southern California Seismic Network and the Southern California Earthquake Data Center for providing

the network data and the IRIS data center and Monica Kohler for providing the LARSE data. We would also like to thank the reviews by Associate Editor Rodolfo Console, Eugene Humphreys, and an anonymous reviewer for the improvement of this manuscript. This research is partially support by USGS contract 04HQAG0010.

References

Abers, G. A., A. Ferris, M. Craig, H. Davies, A. L. Lerner-Lam, J. C. Mutter, and B. Taylor (2002), Mantle compensation of active metamorphic core complexes at Woodlark rift in Papua New Guinea, *Nature*, *418*, 862–865, doi:10.1038/nature00990.

Allmendinger, R. W., J. W. Sharp, D. Vontish, L. Serpa, L. Brown, S. Kaufman, J. Oliver, and R. B. Smith (1983), Cenozoic and Mesozoic structure of the eastern Basin and Range province, Utah, from COCORP seismic reflection data, *Geology*, *11*(9), 526–532.

Allmendinger, R. W., T. A. Hauge, E. C. Hauser, C. J. Potter, S. L. Klemperer, K. D. Nelson, P. Knuepfer, and J. Oliver (1987), Overview of the COCORP 40°N transect, western United States—The fabric of an orogenic belt, *Geol. Soc. Am. Bull.*, *98*(3), 308–319.

Ammon, C. J., G. E. Randall, and G. Zandt (1990), On the nonuniqueness of receiver function inversions, *J. Geophys. Res.*, *95*(B10), 15,303–15,318.

Blakely, R. J., R. C. Jachens, J. P. Calzia, and V. E. Langenheim (1999), Cenozoic basins of the Death Valley extended terrane as reflected in regional-scale gravity anomalies, *Spec. Pap. Geol. Soc. Am.*, *33*, 1–16.

Cassidy, J. F. (1992), Numerical experiments in broad-band receiver function-analysis, *Bull. Seismol. Soc. Am.*, *82*(3), 1453–1474.

Cheadle, M. J., B. L. Czuchra, T. Byrne, C. J. Ando, J. E. Oliver, L. D. Brown, S. Kaufman, P. E. Malin, and R. A. Phinney (1986), The deep crustal structure of the Mojave Desert, California, from COCORP seismic reflection data, *Tectonics*, *5*(2), 293–320.

de Voogd, B., L. Serpa, L. Brown, E. Hauser, S. Kaufman, J. Oliver, B. W. Troxel, J. Willemin, and L. A. Wright (1986), Death Valley bright spot—A midcrustal magma body in the southern Great Basin, California, *Geology*, *14*(1), 64–67.

de Voogd, B., L. Serpa, and L. Brown (1988), Crustal extension and magmatic processes—COCORP profiles from Death Valley and the Rio Grande rift, *Geol. Soc. Am. Bull.*, *100*(10), 1550–1567.

Dibblee, T. W. (1982a), Regional geology of the Transverse Ranges Province of Southern California, in *Geology and Mineral Wealth of the California Transverse Ranges*, vol. 10, edited by D. L. Fife and J. A. Minch, pp. 7–26, South Coast Geol. Soc., Santa Ana, Calif.

Dibblee, T. W. (1982b), Geology of the San Gabriel Mountains, southern California, in *Geology and Mineral wealth of the California Transverse Ranges*, vol. 10, edited by D. L. Fife and J. A. Minch, pp. 131–147, South Coast Geol. Soc., Santa Ana, Calif.

Dokka, R. K., and T. M. Ross (1995), Collapse of southwestern North America and the evolution of early Miocene detachment faults, metamorphic core complexes, the Sierra Nevada Orocline, and the San Andreas fault system, *Geology*, *23*(12), 1075–1078.

Ehlig, P. L. (1981), Origin and Tectonic history of the basement terrane of the San Gabriel Mountains, Central Transverse Ranges, in *The Geotectonic Development of California*, Rubey Vol. vol. I, edited by W. G. Ernst, pp. 253–283, Prentice-Hall, Upper Saddle River, N. J.

Fliedner, M. M., S. L. Klemperer, and N. I. Christensen (2000), Three-dimensional seismic model of the Sierra Nevada arc, California, and its implications for crustal and upper mantle composition, *J. Geophys. Res.*, *105*(B5), 10,899–10,921.

Fuis, G. S., T. Ryberg, N. J. Godfrey, D. A. Okaya, and J. M. Murphy (2001), Crustal structure and tectonics from the Los Angeles basin to the Mojave Desert, southern California, *Geology*, *29*(1), 15–18.

Godfrey, N. J., G. S. Fuis, V. Langenheim, D. A. Okaya, and T. M. Brocher (2002), Lower crustal deformation beneath the central Transverse Ranges, southern California: Results from the Los Angeles Region Seismic Experiment, *J. Geophys. Res.*, *107*(B7), 2144, doi:10.1029/2001JB000354.

Hadley, D. (1978), Geophysical investigations of the structure and tectonics of southern California, Ph.D. thesis, Calif. Inst. of Technol., Pasadena.

Hadley, D., and H. Kanamori (1977), Seismic structure of Transverse Ranges, California, *Geol. Soc. Am. Bull.*, *88*(10), 1469–1478.

Hadley, D., and H. Kanamori (1979), Regional S-wave structure for southern California from the analysis of teleseismic Rayleigh-waves, *Geophys. J. R. Astron. Soc.*, *58*(3), 655–666.

Hauge, T. A., et al. (1987), Crustal structure of western Nevada from COCORP deep seismic reflection data, *Geol. Soc. Am. Bull.*, *98*(3), 320–329.

Hauksson, E. (2000), Crustal structure and seismicity distribution adjacent to the Pacific and North America plate boundary in southern California, *J. Geophys. Res.*, *105*(B6), 13,875–13,903.

Hauksson, E., and J. S. Haase (1997), Three-dimensional V_P and V_P/V_S velocity models of the Los Angeles basin and central Transverse Ranges, California, *J. Geophys. Res.*, *102*(B3), 5423–5453.

Hauser, E., C. Potter, T. Hauge, S. Burgess, S. Burtch, J. Mutschler, R. Allmendinger, L. Brown, S. Kaufman, and J. Oliver (1987), Crustal structure of eastern Nevada from COCORP deep seismic reflection data, *Geol. Soc. Am. Bull.*, *99*(6), 833–844.

Hearn, T. M., and R. W. Clayton (1986a), Lateral velocity variations in southern California. 1. Results for the upper crust from Pg waves, *Bull. Seismol. Soc. Am.*, *76*(2), 495–509.

Hearn, T. M., and R. W. Clayton (1986b), Lateral velocity variations in Southern California. 2. Results for the lower crust from Pn waves, *Bull. Seismol. Soc. Am.*, *76*(2), 511–520.

Houseman, G. A., E. A. Neil, and M. D. Kohler (2000), Lithospheric instability beneath the Transverse Ranges of California, *J. Geophys. Res.*, *105*(B7), 16,237–16,250.

Humphreys, E. D. (1995), Postlaramide removal of the Farallon slab, western United States, *Geology*, *23*(11), 987–990.

Humphreys, E. D., and R. W. Clayton (1990), Tomographic image of the Southern California mantle, *J. Geophys. Res.*, *95*(B12), 19,725–19,746.

Humphreys, E. D., and B. H. Hager (1990), A kinematic model for the late Cenozoic development of southern California crust and upper mantle, *J. Geophys. Res.*, *95*(B12), 19,747–19,762.

Humphreys, E., R. W. Clayton, and B. H. Hager (1984), A tomographic image of mantle structure beneath southern California, *Geophys. Res Lett.*, *11*(7), 625–627.

Ichinose, G., S. Day, H. Magistrale, T. Prush, F. Vernon, and A. Edelman (1996), Crustal thickness variations beneath the peninsular ranges, southern California, *Geophys. Res Lett.*, *23*(22), 3095–3098.

Jennings, C. W. (1975), Fault map of California with locations of volcanoes, thermal springs, and thermal wells, Calif. Div. of Mines and Geol., Sacramento.

Jennings, C. W. (1977), Geologic map of California, Williams & Heintz Map Corp., Capitol Heights, Md.

Jennings, C. W., and J. S. George (1994), Fault activity map of California and adjacent areas, with locations and ages of recent volcanic eruptions, scale 1:750 000, Calif. Dep. of Conserv., Div. of Mines and Geol., Sacramento.

Jones, C. H., and R. A. Phinney (1998), Seismic structure of the lithosphere from teleseismic converted arrivals observed at small arrays in the southern Sierra Nevada and vicinity, California, *J. Geophys. Res.*, *103*(B5), 10,065–10,090.

Kaufman, P. S., and L. H. Royden (1994), Lower crustal flow in an extensional setting: Constraints from the Halloran Hills region, eastern Mojave Desert, California, *J. Geophys. Res.*, *99*(B8), 15,723–15,739.

Kikuchi, M., and H. Kanamori (1982), Inversion of complex body waves, *Bull. Seismol. Soc. Am.*, *72*(2), 491–506.

Kohler, M. D. (1999), Lithospheric deformation beneath the San Gabriel Mountains in the southern California Transverse Ranges, *J. Geophys. Res.*, *104*(B7), 15,025–15,041.

Kohler, M. D., and P. M. Davis (1997), Crustal thickness variations in southern California from Los Angeles Region Seismic Experiment passive phase teleseismic travel times, *Bull. Seismol. Soc. Am.*, *87*(5), 1330–1344.

Langenheim, V. E. (1999), Gravity and aeromagnetic models along the Los Angeles region seismic experiment (LARSE I), California, *U.S. Geol. Surv, Open File Rep., 99-388*.

Langston, C. A. (1977), Effect of planar dipping structure on source and receiver responses for constant ray parameter, *Bull. Seismol. Soc. Am.*, *67*(4), 1029–1050.

Langston, C. A. (1989), Scattering of teleseismic body waves under Pasadena, California, *J. Geophys. Res.*, *94*(B2), 1935–1951.

Lewis, J. L., S. M. Day, H. Magistrale, J. Eakins, and F. Vernon (2000), Regional crustal thickness variations of the Peninsular Ranges, southern California, *Geology*, *28*(4), 303–306.

Lewis, J. L., S. M. Day, H. Magistrale, R. R. Castro, L. Astiz, C. Rebollar, J. Eakins, F. L. Vernon, and J. N. Brune (2001), Crustal thickness of the peninsular ranges and gulf extensional province in the Californias, *J. Geophys. Res.*, *106*(B7), 13,599–13,611.

Li, Y. G., T. L. Henyey, and P. C. Leary (1992), Seismic reflection constraints on the structure of the crust beneath the San Bernardino Mountains, Transverse Ranges, southern California, *J. Geophys. Res.*, *97*(B6), 8817–8830.

Ligorria, J. P., and C. J. Ammon (1999), Iterative deconvolution and receiver function estimation, *Bull. Seismol. Soc. Am.*, *89*(5), 1395–1400.

Owens, T. J., and G. Zandt (1985), The response of the continental crust-mantle boundary observed on broad-band teleseismic receiver functions, *Geophys Res. Lett.*, *12*(10), 705–708.

Pellerin, C. L. M., and N. I. Christensen (1998), Interpretation of crustal seismic velocities in the San Gabriel-Mojave region, southern California, *Tectonophysics*, *286*(1-4), 253–271.

Peng, X. H., and E. D. Humphreys (1997), Moho dip and crustal anisotropy in northwestern Nevada from teleseismic receiver functions, *Bull. Seismol. Soc. Am.*, *87*(3), 745–754.

Richards-Dinger, K. B., and P. M. Shearer (1997), Estimating crustal thickness in southern California by stacking PmP arrivals, *J. Geophys. Res.*, *102*(B7), 15,211–15,224.

Ryberg, T., and G. S. Fuis (1998), The San Gabriel mountains bright reflective zone: Possible evidence of young mid-crustal thrust faulting in southern California, *Tectonophysics*, *286*(1-4), 31–46.

Savage, M. K. (1998), Lower crustal anisotropy or dipping boundaries? Effects on receiver functions and a case study in New Zealand, *J. Geophys. R.*, *103*(B7), 15,069–15,087.

Snow, J. K., and B. P. Wernicke (2000), Cenozoic tectonism in the central basin and range: Magnitude, rate, and distribution of upper crustal strain, *Am. J. Sci.*, *300*(9), 659–719.

Wang, K., T. Plank, J. D. Walker, and E. I. Smith (2002), A mantle melting profile across the Basin and Range, SW USA, *J. Geophys. Res.*, *107*(B1), 2017, doi:10.1029/2001JB000209.

Wooley, R. J., and V. E. Langenheim (2001), Gravity data along LARSE (Los Angeles Region Seismic Experiment) II, Southern California, *U.S. Geol. Surv. Open File Rep., 01-375*.

Yan, Z. (2007), Regional mapping of the crustal structure in southern California, Ph.D. thesis, Calif. Inst. of Technol., Pasadena.

Zhu, L. P. (2000), Crustal structure across the San Andreas Fault, southern California from teleseismic converted waves, *Earth Planet. Sci. Lett.*, *179*(1), 183–190.

Zhu, L. P. (2002), Deformation in the lower crust and downward extent of the San Andreas Fault as revealed by teleseismic waveforms, *Earth Planets Space*, *54*(11), 1005–1010.

Zhu, L. P., and H. Kanamori (2000), Moho depth variation in southern California from teleseismic receiver functions, *J. Geophys. Res.*, *105*(B2), 2969–2980.

R. W. Clayton, MS 252-21, Seismological Laboratory, California Institute of Technology, Pasadena, CA 91125, USA. (clay@gps.caltech.edu)

Z. Yan, WesternGeco, 10001 Richmond Ave., Houston, TX 77042, USA. (zhimei@gmail.com)